Acta Pharmaceutica Sinica B 2026;16(6):3764−3783

Chinese Pharmaceutical Association
Institute of Materia Medica, Chinese Academy of Medical Sciences

Acta Pharmaceutica Sinica B

www.elsevier.com/locate/apsb
www.sciencedirect.com

ORIGINAL ARTICLE

Lactate metabolism and epigenetic reprogramming drive c-KIT hyperactivation to mediate Gilteritinib resistance: Rationale for c-KIT degraders over kinase inhibitors

Yanli Zhao[a,†], Yubo Wang[a,†], Ning Liu[a], Yijie Yang[a], Jialu Li[a], Ziqi Huang[a,*], Lan Ma[a,*], Shuang Yang[a,*], Shuangwei Liu[a,*], Jingfeng Zhou[b,*], Guang Yang[a,*]

[a]*The State Key Laboratory of Medicinal Chemical Biology, College of Pharmacy, Nankai University, Tianjin 300071, China*
[b]*Department of Hematology and Oncology, International Cancer Center, Shenzhen Key Laboratory of Precision Medicine for Hematological Malignancies, Shenzhen University General Hospital, Shenzhen University Clinical Medical Academy, Shenzhen University Health Science Center, Shenzhen 518000, China*

Received 5 August 2025; received in revised form 11 December 2025; accepted 12 December 2025

KEY WORDS

FLT3-ITD;
Gilteritinib;
Drug resistance;
c-KIT;
Targeted protein degradation;
Lactate metabolism reprogramming;
PDX

Abstract Kinase inhibitors targeting FLT3-ITD, such as Gilteritinib, have emerged as promising targeted therapies. However, recent clinical trials have shown disappointing overall survival (OS) outcomes in acute myeloid leukemia (AML) patients, primarily due to disease recurrence following treatment. We uncovered a potential mechanism underlying Gilteritinib resistance. Gilteritinib treatment induced reprogramming of lactic acid metabolism in AML cells, leading to increased H3K27 lactylation that continuously amplified c-KIT expression and signaling in AML cells. This mechanism enriched leukemia stem cells (LSCs), driving drug resistance and disease relapse. Notably, c-KIT kinase inhibitors failed to effectively counteract the progression of relapsed and refractory AML, as c-KIT overexpression results in amplification of its signaling. To address this issue, a dual degrader targeting both FLT3-ITD and c-KIT was identified. Beyond exhibiting stronger efficacy than Gilteritinib in inhibiting AML cell proliferation, this PROTAC also demonstrates a significant ability to induce cell differentiation. In cell line-derived xenograft (CDX) models, the degrader significantly suppressed FLT3-ITD^{+} AML recurrence

*Corresponding authors.
E-mail addresses: 9920250119@nankai.edu.cn (Ziqi Huang), 1120220728@mail.nankai.edu.cn (Lan Ma), yangshuang@nankai.edu.cn (Shuang Yang), shuangwei.liu@nankai.edu.cn (Shuangwei Liu), jingfengzhou@szu.edu.cn (Jingfeng Zhou), Guang.yang@nankai.edu.cn (Guang Yang).
[†]These authors made equal contributions to this work.
Peer review under the responsibility of Chinese Pharmaceutical Association and Institute of Materia Medica, Chinese Academy of Medical Sciences.

https://doi.org/10.1016/j.apsb.2026.01.045

and prolonged the survival of experimental mice. Furthermore, in PDX model established using AML cells from Gilteritinib-resistant patients, the degrader showed significantly superior therapeutic efficacy compared to the combination treatment of Gilteritinib and Imatinib. As a candidate drug molecule, this degrader exhibits promising potential for clinical translation.

1. Introduction

Acute myeloid leukemia (AML) is an extremely aggressive and diverse hematological cancer. Its incidence is remarkably high, especially among the elderly[1]. The root cause of AML lies in the disrupted differentiation of normal hematopoietic stem cells (HSCs). This disruption is triggered by the abnormal growth and spread of immature myeloid cells inside the bone marrow[2]. When AML starts, it's often accompanied by changes in chromosome arrangements and gene mutations[3]. Among these genetic changes, mutations in the fms-related receptor tyrosine kinase 3 (FLT3) gene are the most common triggers in AML. These mutations are found in over 30% of all AML patients[4]. FLT3 mutations mainly include internal tandem duplication (ITD) either in or near the juxtamembrane region, as well as point mutations in its tyrosine kinase domain (TKD)[5]. FLT3-ITD causes the continuous activation of signals that prevent cell death, support cell survival, and encourage cell growth in myeloid leukemic cells. Because of these effects at the molecular level, FLT3-ITD has become a very promising target for creating drugs to treat AML in the clinic[6].

Gilteritinib, a novel-generation FLT3-ITD inhibitor, exhibits remarkable inhibitory potency and selectivity. It has recently received US Food and Drug Administration (FDA) approval for the treatment of FLT3-ITD-positive AML[7]. Emerging evidence suggests that while Gilteritinib, as well as other FLT3-ITD inhibitors, can swiftly eliminate leukemic cells in the peripheral blood. However, the minimal residual AML cells persist in the bone marrow, which may potentially trigger a relapse[8-12]. Initially, most patients demonstrate a favorable response to these drugs and achieve rapid complete hematological remission. Nevertheless, drug resistance invariably emerges, leading to AML recurrence within a few months[13]. In recent years, several promising FLT3 inhibitors have been approved by the FDA or are undergoing clinical trials[14-16]. However, clinical outcomes demonstrate that they still fail to prevent AML recurrence[17,18]. These results indicate that simply enhancing drug selectivity and inhibitory activity toward FLT3 kinase is insufficient to overcome AML relapse following FLT3-targeted therapy. More critically, the mechanisms underlying acquired resistance to FLT3i-treatment remain largely undefined[19-23]. This gap in mechanistic understanding has hindered the development of innovative targeted intervention strategies. In this study, we conduct an integrated multi-omics analysis using clinical patient samples and AML cell lines to elucidate the mechanisms underlying Gilteritinib resistance. Based on these findings, we aim to develop innovative and alternative targeted intervention strategies and discover the drug candidate for the treatment of FLT3-ITD-positive AML.

2. Results

As mentioned in the introduction, multiple clinical investigations have demonstrated that the majority of patients treated with Gilteritinib (Fig. 1A) experience rapid relapse of AML[10]. Consequently, elucidating the mechanism of Gilteritinib resistance has emerged as a critical scientific challenge in clinical translational research. To explore the underlying mechanism of AML resistance and relapse, we intially treated two FLT3-ITD-positive AML cell lines, MOLM-13 and MV-4-11, with Gilteritinib *in vitro*. As presented in Fig. 1B, Gilteritinib treatment effectively suppressed the downstream signaling of FLT3-ITD. It significantly decreased the phosphorylation levels of FLT3-ITD, STAT5, STAT3, and AKT in dose-dependent manners. To be noticed, it was revealed that Gilteritinib failed to inhibit the ERK signaling pathway. Instead, with an increase in dosage, the treatment activated the ERK signaling pathway in the surviving AML cells (Fig. 1B). This is consistent with many previous findings from clinical studies[24-26]. Fortunately, we obtained paired samples from an AML patient who relapsed after Gilteritinib treatment (both pre-treatment and post-relapse) and conducted transcriptomic analyses. Comparing the Gilteritinib group with the control group, a Gene Set Enrichment Analysis (GSEA) analysis was performed to study on the pathways that significantly affected the ERK signaling. It was indicated that, compared to the control group, cells treated with Gilteritinib could significantly influence stem cells differentiation, growth factor binding, and Ras signaling (Fig. 1C). Next, we further performed a venn analysis on the differentially expressed genes related to these pathways. Notably, it was identified a common significantly differentially expressed gene, c-KIT (Fig. 1D). Additionally, it was observed a distinct upregulation of c-KIT at the transcriptional level (Fig. 1E). Recent preclinical and clinical studies have highlighted that c-KIT is not only identified as a promising biomarker of LSCs in AML but also plays a crucial role in regulating LSCs self-renewal[27-31]. Validation by quantitative real-time polymerase chain reaction (qPCR) and Western blotting demonstrated that Gilteritinib treatment significantly increased both the expression and phosphorylation levels of c-KIT in FLT3-ITD$^+$ AML cell lines (Fig. 1F and G). Additionally, primary blood samples were collected from healthy individuals and FLT3-ITD$^+$ AML patients. And c-KIT transcriptional levels were analyzed. As shown in Fig. 1H, c-KIT expression was significantly higher in the blood samples of AML patients compared to healthy controls. Notably, the c-KIT transcription levels were highest in patients who relapsed after Gilteritinib treatment, which is consistent with our previous *in vitro* results. Detailed clinical information of these Gilteritinib-resistant patients is provided in Supporting Information Table S1. Overall, these results indicate that treating AML cells with Gilteritinib can probably enrich and activate LSCs by upregulating c-KIT expression as well as ERK phosphorylation, potentially contributing to treatment failure and AML relapse.

Meanwhile, to delve deeper into the impacts of Gilteritinib treatment on AML cells, metabolomics studies were simultaneously conducted (Supporting Information Fig. S1). According

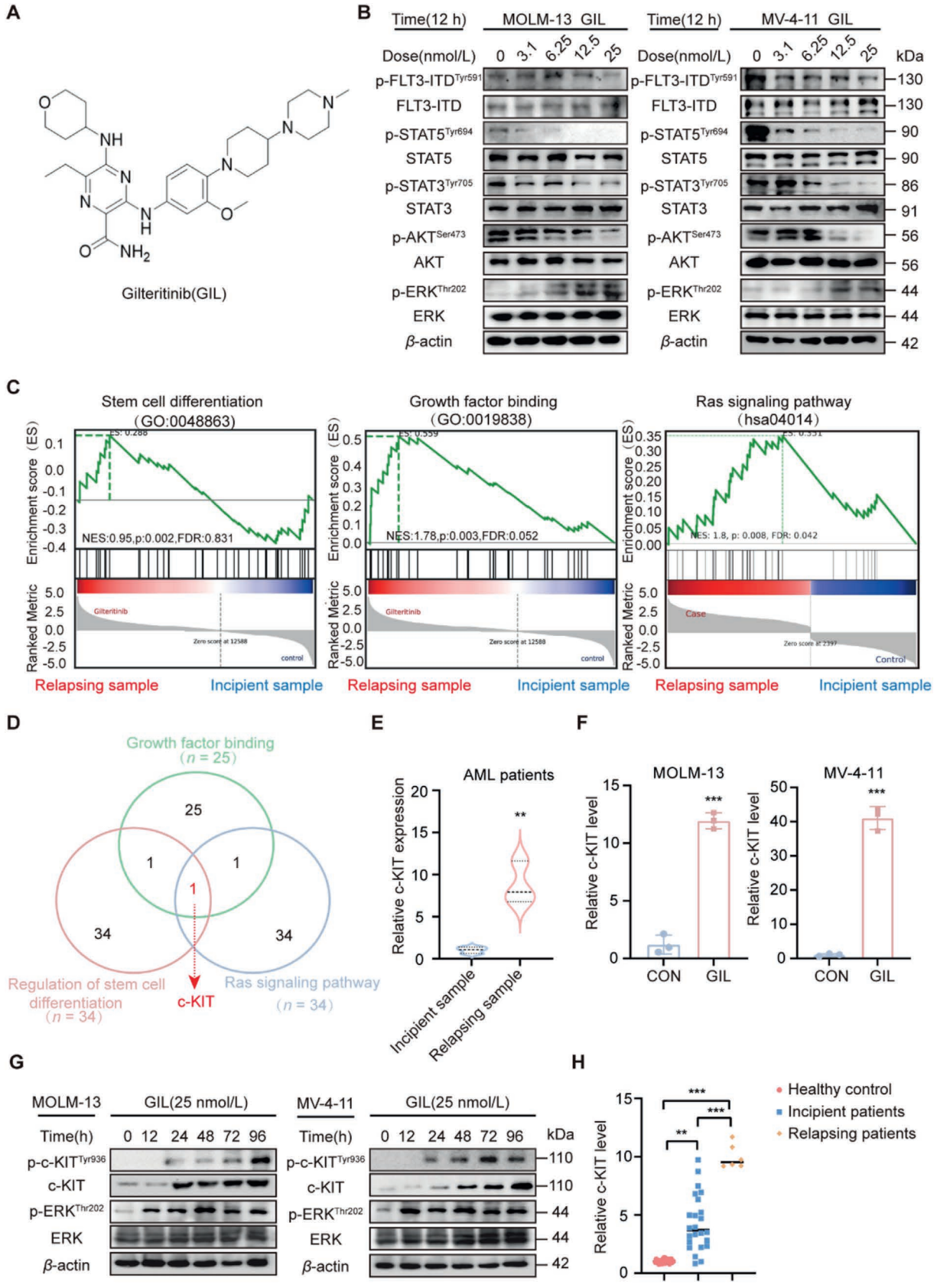

Figure 1 Gilteritinib treatment elevates the transcriptional level of c-KIT in AML cells. (A) Chemical structure of Gilteritinib. (B) Immunoblot assay of p-FLT3, p-STAT5, p-AKT, and p-ERK protein levels in MOLM-13 and MV-4-11 cells treated with a concentration gradient of Gilteritinib for 12 h. (C) GSEA enrichment plot of stem cell differentiation, growth factor binding, and Ras signaling pathway using RNA-seq data generated

to untargeted metabolomics results, several fatty acids were found to be uptaken differentially in Gilteritinib-treatment group, comparison with the vehicle group (Fig. 2A)[32,33]. Notably, we paid particular attention to a significant increase in lactic acid uptake after Gilteritinib treatment. This result was also confirmed by quantitative testing of cellular lactic acid (Fig. 2B and Fig. S1A). The transcriptomic data were then investigated to analyze the differentially expressed genes associated with lactic acid transport and utilization. To our surprise, following Gilteritinib treatment, the transcriptional levels of monocarboxylate transporter 3 (MCT3)[34,35] and lactyl-CoA synthetase short-chain family member 2 (ACSS2)[36,37] were uncovered to be significantly elevated (Fig. 2C and Fig. S1B). Subsequently, the expression of ACSS2 and MCT3 were validated in two FLT3-ITD$^+$ AML cell lines, MV-4-11 and MOLM-13 cells, using qPCR and Western blotting. The results confirmed that MCT3 and ACSS2 were both transcriptionally upregulated remarkably, after treated with Gilteritinib (Fig. 2D and E, and Fig. S1C and S1D). Next, the cellular levels of lactyl-CoA were quantitatively evaluated in both AML cell lines. Compared to the control group, AML cells in the Gilteritinib-treated group showed a distinct cellular accumulation of lactyl-CoA (Fig. 2F).

To investigate the impact of lactates on AML cells, we supplemented the culture medium of AML cells with different concentrations of lactate. Firstly, it was found that the presence of lactates could significantly promote the proliferation of two FLT3-ITD$^+$ AML cell lines (Fig. 2G and Fig. S1E). Meanwhile, the results of the soft-agar colony formation assay demonstrated that lactates could significantly increase the number of malignant colonies of AML cells (Fig. 2H and Fig. S1F). Moreover, CCK8 assay results further revealed that lactate supplementation markedly attenuated the cytotoxicity of Gilteritinib in AML cells (Fig. 2I), indicating that exogenous lactate confers resistance to Gilteritinib treatment. In conclusion, Gilteritinib treatment could trigger metabolic reprogramming in AML cells, prominently enhancing the uptake of lactates. High cellular level of lactates promoted proliferation of AML cells. This may represent the primary mechanism driving acquired resistance in AML cells.

Recent multiple important studies have focused on the critical regulatory role of lactyl-CoA in the epigenetic modification of proteins, governing their stability and activity[38]. Notably, the level of histone lactylation can modify chromatin morphology, subsequently influencing mRNA transcription[39-41]. We hypothesized that the intracellular accumulation of lactyl-CoA could increase the lactylation level of histone at specific sites to activate the c-KIT, ACSS2, MCT3 gene promoter region. To authenticate this, Western blotting experiments were firstly employed to evaluate the lactylation levels at various sites of histones (Fig. 3A, Supporting Information Fig. S2A and S2B). As anticipated, Gilteritinib treatment significantly increased the lactylation levels of H3 at previously reported sites (Fig. 3A, and Fig. S2A) [42]. Next, chromatin immunoprecipitation (ChIP) experiments were performed to identify the specific lactylation sites of H3 that would be located in the c-KIT promoter region (Fig. 3B, and Fig. S2C). The CHIP-qPCR results revealed that only the H3K27la could be significantly enriched in the c-KIT promoter region (Fig. 3B, and Supporting Information Fig. S3A). Meanwhile, lactate nutritional intervention experiments were conducted to evaluate their impact on the aforementioned genes and their downstream signaling pathways. The results demonstrated the following: first, lactate significantly upregulated the level of H3K27 lactylation modification, activated the transcriptional and protein expression of ACSS2, MCT3, and c-KIT, and notably increased the phosphorylation levels of c-KIT and ERK, all of which exhibited a significant time-dependent pattern (Fig. 3C and D). Additionally, the intracellular synthesis of lactyl-CoA was markedly enhanced (Fig. 3E). More notably, further ChIP-qPCR experimental results revealed that H3K27la could also be enriched in the promoter regions of ACSS2 and MCT3 (Fig. 3F, G and Fig. S3B and S3C). These findings suggest that Gilteritinib-mediated lactate metabolic reprogramming-induced H3K27la modification could activate the promoter regions of c-KIT, ACSS2, and MCT3, transcriptionally upregulate the expression of these genes, and thereby promote the transduction of c-KIT downstream LCSs signaling, as well as the uptake of lactate and the synthesis of lactyl-CoA.

To further clarify the molecular mechanism underlying Gilteritinib-induced c-KIT transcription upregulation, AML cell lines with either ACSS2 knockdown or overexpression were generated. The results of qPCR and Western blotting indicated that, compared to the vector group, ACSS2 knockdown led to a decrease in c-KIT expression and the phosphorylation levels of c-KIT and ERK (Fig. 4A and C). In contrast, ACSS2 overexpression significantly elevated the levels of c-KIT, p-c-Kit, and p-ERK (Fig. 4B and D). Moreover, more intervention experiments were conducted for further mechanical validation. The results indicated that knocking down ACSS2, or inhibiting ACSS2 with MTB-9655, or inhibiting EP300 (the histone lactoyltransferases) with C646 all blocked the Gilteritinib-mediated upregulation of Ac-H3K27, c-KIT, p-c-KIT, and p-ERK levels in both AML cell lines (Fig. 4E). These findings provided further evidence to proof our hypothesis. Additionally, we also explored that whether activation of c-KIT down-stream signaling could activate transcripnal expression of ACSS2 and MCT3 (Fig. 4F−I). The *c-KIT*-alterated AML cells lines were then establised. Moreover, the further experimental results demonstrated that c-KIT overexpression could significantly enhanced lactate uptake and promoted lactyl-CoA accumulation in AML cells (Supporting Information Fig. S4). In summary, a plausible mechanism has been uncovered (Fig. 4J). Gilteritinib-induced stress triggered lactate metabolic reprogramming in AML cells, obliged them to preferentially uptake lactic acid and produced higher intracellular amount of lactyl-CoA. This, in turn, elevated the level of H3K27la, leading to the activation of chromatin in the c-KIT promoter region and amplified c-KIT expression. Moreover, it was further verified that H3K27la modification can transcriptionally activate both ACSS2 and MCT3 simultaneously. This epigenetic change enhances the uptake and utilization of lactate by AML cells, and through a positive feedback loop mechanism, further amplifies the

from incipient sample, and relapsing sample of the AML patients. (D) Venn diagram shows the communication of genes contained in the three signaling pathways. (E) Expression of c-KIT using RNA-seq data generated from incipient sample, and relapsing sample of the AML patients. (F) Evaluation of c-KIT mRNA levels in AML cells treated with 25 nmol/L of Gilteritinib for 24 h, using qRT-PCR. (G) Evaluation of p-c-KIT, p-ERK protein levels in AML cells treated with 25 nmol/L of Gilteritinib for different times, using Western blot. (H) Evaluation of c-KIT mRNA levels in AML patients using qRT-PCR. Quantitative data were summarized from three independent replicate experiments and expressed as mean ± SD, $^{**}P < 0.01$, $^{***}P < 0.001$ (Student' *t*-test).

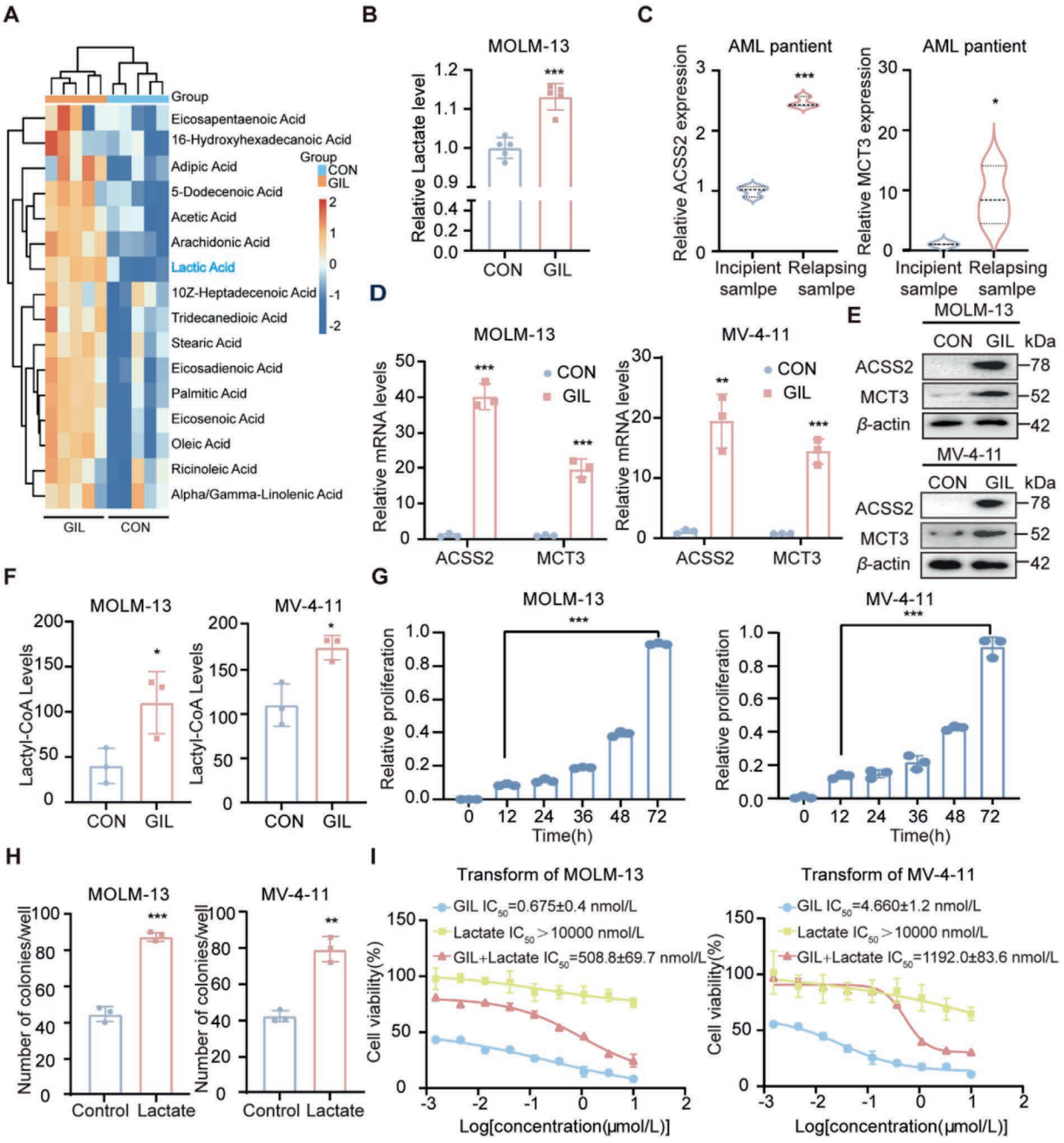

Figure 2 Gilteritinib treatment increases the uptake and utilization of lactic acid in AML cells. (A) Heatmap using untargeted metabolomics data generated from MV-4-11 cells treated with and without Gilteritinib. (B) The content of lactate using triple quadrupole mass spectrometer tested in the AML cells treated with and without Gilteritinib. (C) Expression of ACSS2, and MCT3 using RNA-seq data generated from incipient sample, and relapsing sample of the AML patients. (D) Evaluation of *ACSS2*, and *MCT3* mRNA levels in AML cells treated with 25 nmol/L of Gilteritinib for 24 h, using qRT-PCR. (E) Evaluation of ACSS2, and MCT3 protein levels in AML cells treated with 25 nmol/L of Gilteritinib for 24 h, using Western blot. (F) The content of lactyl-CoA using triple quadrupole mass spectrometer tested in the AML cells treated with and without Gilteritinib. (G) Cell growth curve of AML cells treated with 0.5 mmol/L lactate. (H) Determination of colony-forming units (CFU) of MOLM-13 and MV-4-11 cells treated with lactate. (I) Detection by CCK-8 shows the effect of lactate on AML cell proliferation. Quantitative data were summarized from three independent replicate experiments and expressed as mean ± SD, $^{*}P < 0.05$, $^{**}P < 0.01$, $^{***}P < 0.001$ (Student' *t*-test).

transcription of c-KIT and the activation of its downstream signaling. It consequentially led to the enrichment of LSCs in AML cells, contributing to drug resistance and relapse of AML cells after Gilterinitb targeted therapy.

Based on the results of the proposed mechanism, it was postulated that continuous inhibition of FLT3-ITD in AML cells might gradually cause the accumulation of c-KIT. This accumulation leads to a substantial enrichment of leukemia stem cells

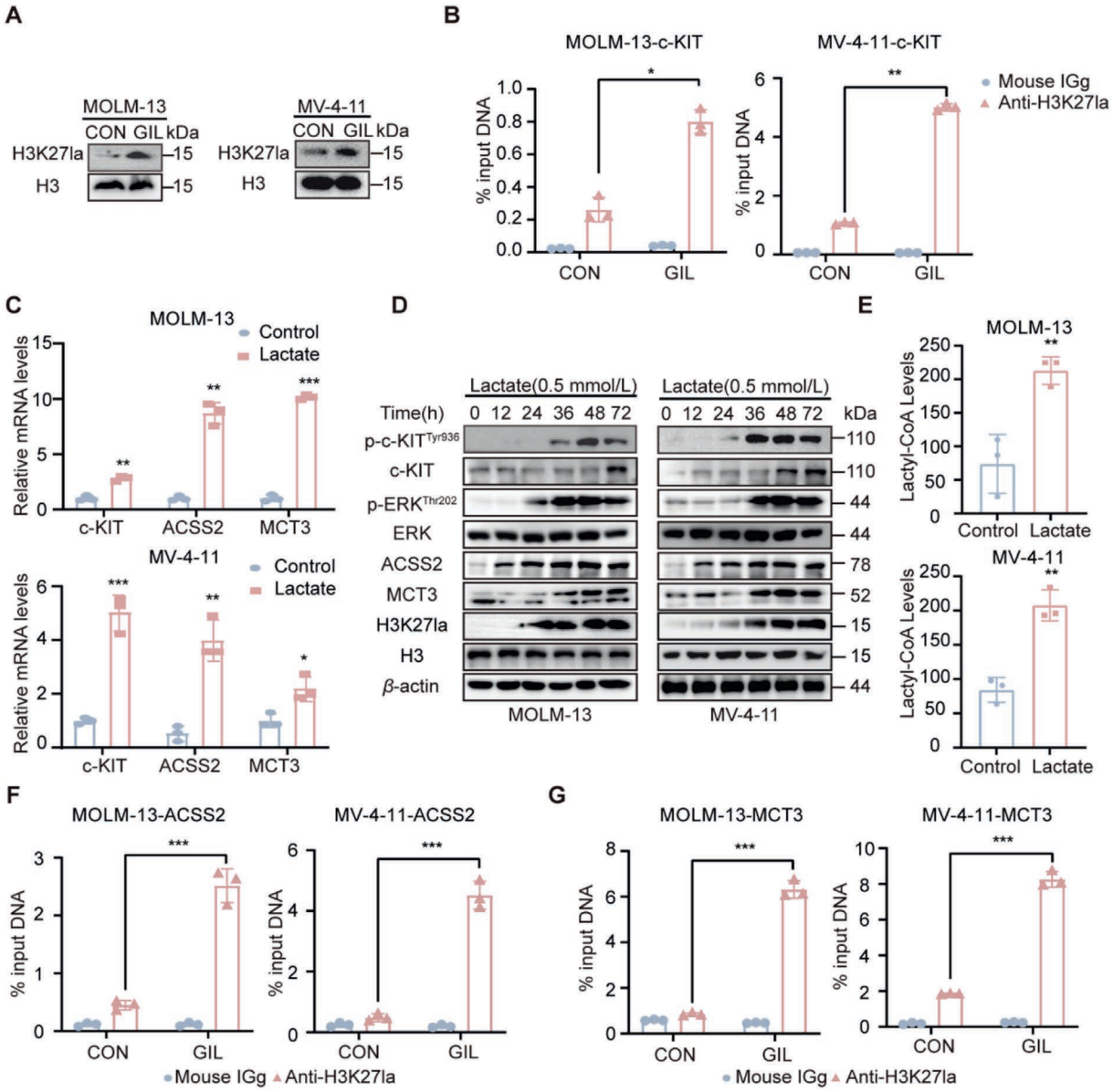

Figure 3 Screening of histone lactylation sites. (A) Evaluation of H3K27la protein levels in AML cells treated with 25 nmol/L of Gilteritinib for 24 h, using Western blot. (B) The binding of H3K27la protein on the c-KIT gene promoter in AML cells treated with and without Gilteritinib determined by ChIP-qPCR assays. (C) Evaluation of c-KIT, ACSS2, and MCT3 mRNA levels in AML cells treated with 0.5 mmol/L lactate for 24 h, using qRT-PCR. (D) Evaluation of p-c-KIT, p-ERK, ACSS2, MCT3, and H3K27la protein levels in AML cells treated with 0.5 mmol/L lactate for time gradient, using Western blot. (E) The content of lactyl-CoA using triple quadrupole mass spectrometer tested in the AML cells treated with and without lactate. (F) The binding of H3K27la protein on the ACSS2 gene promoter in AML cells treated with and without Gilteritinib determined by ChIP-qPCR assays. (G) The binding of H3K27la protein on the MCT3 gene promoter in AML cells treated with and without Gilteritinib determined by ChIP-qPCR assays. Quantitative data were summarized from three independent replicate experiments and expressed as mean ± SD, $^{*}P < 0.05$, $^{**}P < 0.01$ (Student' *t*-test).

(LSCs), subsequently resulting in rapid AML relapse. This further logically explains why current promising FLT3 kinase inhibitors inevitably lead to AML relapse: they fail to completely suppress the continuously amplified c-KIT signaling following epigenetic reprogramming. In fact, clinical researchers have observed the phenomenon we identified: treatment with FLT3 inhibitors and other drugs can lead to c-KIT upregulation, transforming AML into a relapsed and refractory form. Consequently, clinical studies attempting combination therapy with FLT3 and c-KIT inhibitors have failed to obtain FDA approval, due to the lack of a significant reduction in relapse rates and significantly increased bone marrow toxicity[43,44]. Our study appears to reveal a potential mechanism: c-KIT kinase inhibitors are unable to fully alleviate relapsed and refractory AML.

Recently, increasingly mature targeted protein degradation (TPD) technologies, particularly proteolysis-targeting chimeras (PROTACs), offer potential inspiration for addressing this issue[45,46]. We propose that using a PROTAC molecule capable of selectively and potently degrading both FLT3-ITD and c-KIT in AML cells—without affecting these proteins in other normal

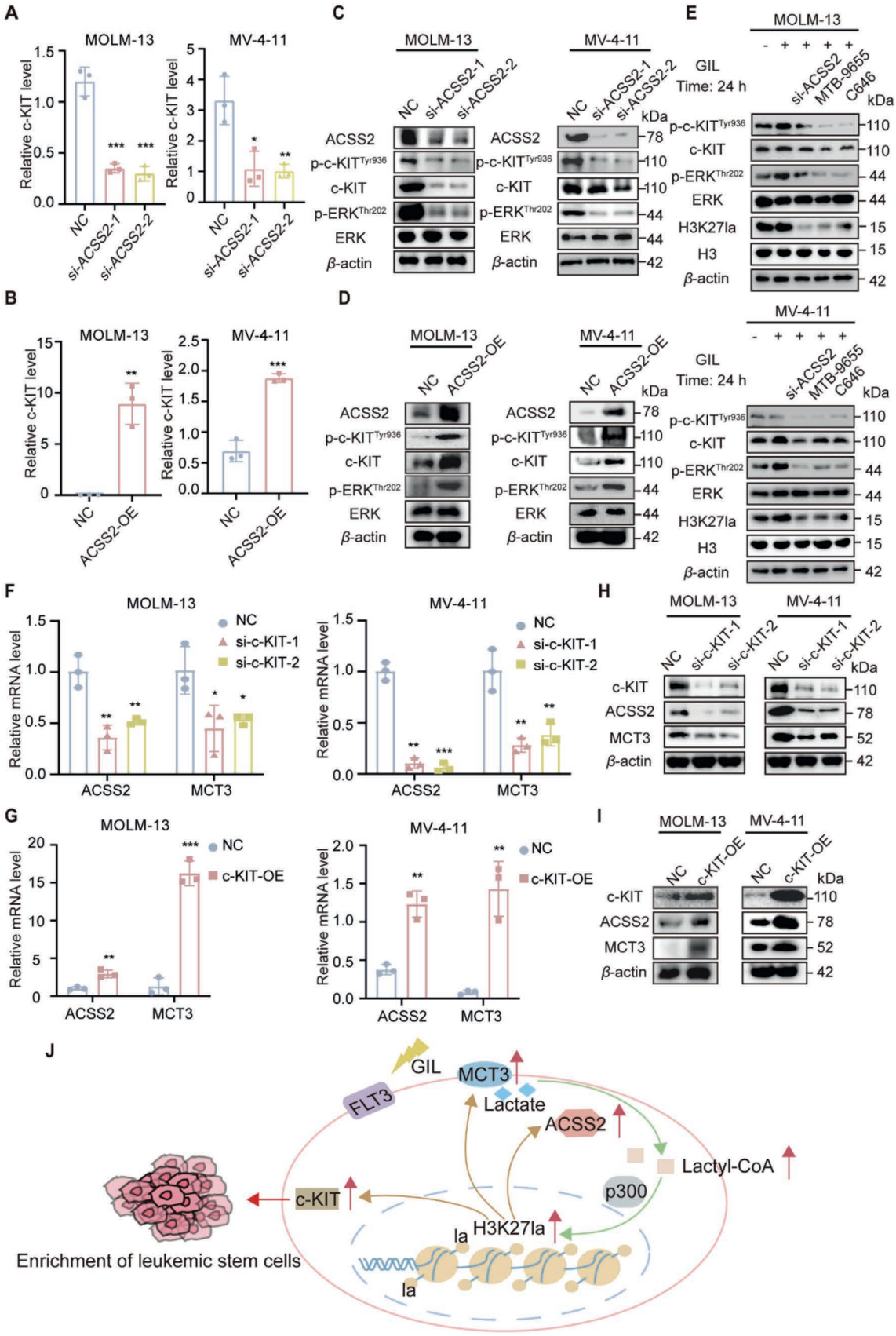

Figure 4 Lactylation of H3K27 upregulates activation of c-KIT transcription. (A) Evaluation of c-KIT mRNA level in si-ACSS2 AML cells, using qRT-PCR. (B) Evaluation of c-KIT mRNA level in ACSS2-OE AML cells, using qRT-PCR. (C) Evaluation of c-KIT and p-ERK protein levels in si-ACSS2 AML cells, using Western blot. (D) Evaluation of c-KIT and p-ERK protein levels in ACSS2-OE AML cells, using Western

hematopoietic stem cells—could completely disrupt the c-KIT-associated regulatory positive-feedback loop and overcome the challenges of gilteritinib-mediated AML resistance and relapse.

To this end, Dovitinib was selected as the ligand for the proteins of interest (POIs) in developing potent degraders (Supporting Information Fig. S5A). This choice was due to its strong binding affinities for both FLT3-ITD and c-KIT. Docking simulations of Dovitinib with the kinase domains of FLT3-ITD and c-KIT indicated that the piperazine group extended outward from the protein pockets of both, suggesting it as the most suitable site for PROTAC structural modification (Fig. S5B)[47]. It has been reported that increasing the rigidity of linkers can regulate and constrain the conformations of molecules, which may facilitate the more efficient and selective formation of ternary complexes[48,49]. Through the principle of PROTAC technology (Fig. S5C), we designed and synthesized compounds **A1**−**A10** (Supporting Information Table S2), whose linkers exhibit higher rigidity than previous reported compounds. Encouragingly, most of these compounds demonstrated enhanced FLT3-ITD degradation efficacy and antiproliferative activity. Among them, compound **A3** showed the most potent FLT3-ITD and c-KIT degradation capability, with excellent IC_{50} values in MV-4-11 and MOLM13 cells ($IC_{50} = 1.262 \pm 0.14$ and 0.1238 ± 0.003 nmol/L, respectively).

Multiple studies have indicated that thalidomide-based PROTAC molecules exhibit poor pharmacokinetic properties, primarily attributed to their high topological polar surface area (TPSA) and susceptibility to hydrolysis[49,50]. It was hypothesized that incorporating thalidomide analogues would be beneficial for enhancing the membrane permeability and oral bioavailability of PROTACs. Therefore, we synthesized compounds **B1**−**B11** (Table S2 and Fig. S5D) featuring optimized linkers and novel cereblon (CRBN) ligand structures. To our delight, Western blotting experiments revealed that compound **B11** ($DC_{50} < 1$ nmol/L in MOLM-13 cell lines) exerted potent effects on target degradation ((Fig. 5A and B). Additionally, we evaluated the antiproliferative activity of **B11** in comparison to its parent scaffold Dovitinib. The results showed that Dovitinib exhibited markedly weaker inhibitory effects on AML cell proliferation, indicating insufficient potency for targeted therapeutic use. In contrast, **B11** demonstrated significantly enhanced cytotoxicity, highlighting the pharmacological advantages conferred by the PROTAC-based degradation strategy (Supporting Information Fig. S6).

To further evaluate the drugability of **B11**, firstly, the preliminary *in vitro* studies on drug metabolism and pharmacokinetics were conducted. It was found that **B11** exhibited excellent metabolic stability in both mouse and human liver microsomes (LMs, Supporting Information Table S3). Meanwhile, the absorption of drug molecules by intestinal epithelial cells depends on their solubility in intestinal fluid[51]. By using FeSSIF buffer to simulate the intestinal fluids, it was found that **B11** had good aqueous solubility (Supporting Information Table S4). These results indicated that **B11** might have adequate oral bioavailability. Therefore, preliminary pharmacokinetic (PK) studies were conducted in mice. Following intravenous administration at 5 mg/kg, **B11** exhibited an AUC of 6430.75 ng h/mL and a C_{max} of 3432.89 ng/mL. After oral dosing at 25 mg/kg, the AUC reached 9432.92 ng h/mL with a C_{max} of 2890.71 ng/mL, corresponding to an oral bioavailability of approximately 30%. These findings suggest that **B11** achieves efficient absorption and systemic exposure following oral administration, supporting its potential for further oral formulation development (Supporting Information Fig. S7). In addition, to investigate whether **B11** has hematotoxicity, a 28-day drug-related factors (DRF) experiment was conducted. The results of the blood routine test demonstrated that continuous administration of **B11** did not significantly cause bone marrow toxicity in the experimental animals (Supporting Information Fig. S8A). More importantly, *in vitro* tests using bone marrow samples from healthy individuals were conducted, and the results elucidated that **B11** at a concentration of 1000 nmol/L did not significantly induce cell death in bone marrow cells (Fig. S8B and S8C). In conclusion, the above experimental results fully indicated that **B11** can be selected as the drug candidate for further pharmacodynamic evaluations.

Western blot experiments revealed that **B11** treatment could rapidly degrade POIs at low drug concentrations in both dose- and time-dependent manners (Fig. 5C−E). To further validate whether the drug molecule mediated POI degradation *via* a PROTACs mechanism, several intervention experiments were carried out *in vitro*. Specifically, pre-treatment with the proteasome inhibitor MG132 or the CRBN inhibitor MLN4924 (MLN) notably inhibited POI degradation. This implies that **B11**-induced POI protein degradation hinged on the both activated proteasome and CRBN. Pre-incubating AML cells with POI and CRBN ligands also significantly suppressed POI degradation, suggesting that **B11**-induced proteins degradation also depended on the formation of the classic ternary complexes involving POIs, CRBN and PROTAC molecule (Fig. 5F). Cycloheximide (CHX) intervention experiments showed that the combination of **B11** and CHX markedly shortened the half-life of the target proteins, providing direct evidence that **B11**-induced POI degradation is reliant on the ubiquitin-proteasome system (Fig. 5G). Subsequently, immunoprecipitation (ip) and Western blot results indicated that the ubiquitination levels of FLT3-ITD and c-KIT proteins were significantly elevated after drug treatment (Fig. 5H). To further evaluate the selectivity of **B11**-induced POI degradation, both kinase panel profiling and quantitative proteomics analyses were performed (Fig. 5I and Supporting Information Fig. S9A). The results indicated that FLT3 and c-KIT were the most prominently degraded proteins upon **B11** treatment. Additionally, distinct degradation of PDGFRβ, another well-known target of Dovitinib, was also detected and subsequently confirmed by Western blot analysis (Fig. S9B). Although PDGFRβ was not the primary focus of this study, its degradation may be advantageous in AML, as reported in previous studies[52-54]. In conclusion, *in vitro* evaluations demonstrated that the PROTACs molecule **B11** effectively mediated the selective and potent degradation of FLT3-ITD and c-KIT *via* the ubiquitin−proteosome pathway.

Blot. (E) Evaluation of p-c-KIT, p-ERK, and H3K27la protein levels in AML cells treated with different treatment conditions for 24 h, using Western blot. (F) Evaluation of *ACSS2* and *MCT3* mRNA levels in si-c-KIT AML cells, using qRT-PCR. (G) Evaluation of *ACSS2* and *MCT3* mRNA levels in c-KIT-OE AML cells, using qRT-PCR. (H) Evaluation of ACSS2, and MCT3 protein levels in si-c-KIT AML cells, using Western blot. (I) Evaluation of ACSS2, and MCT3 protein levels in c-KIT-OE AML cells, using Western blot. (J) Summary of the mechanism diagram. Quantitative data were summarized from three independent replicate experiments and expressed as mean ± SD, $^{*}P < 0.05$, $^{**}P < 0.01$, $^{***}P < 0.001$ (Student' *t*-test).

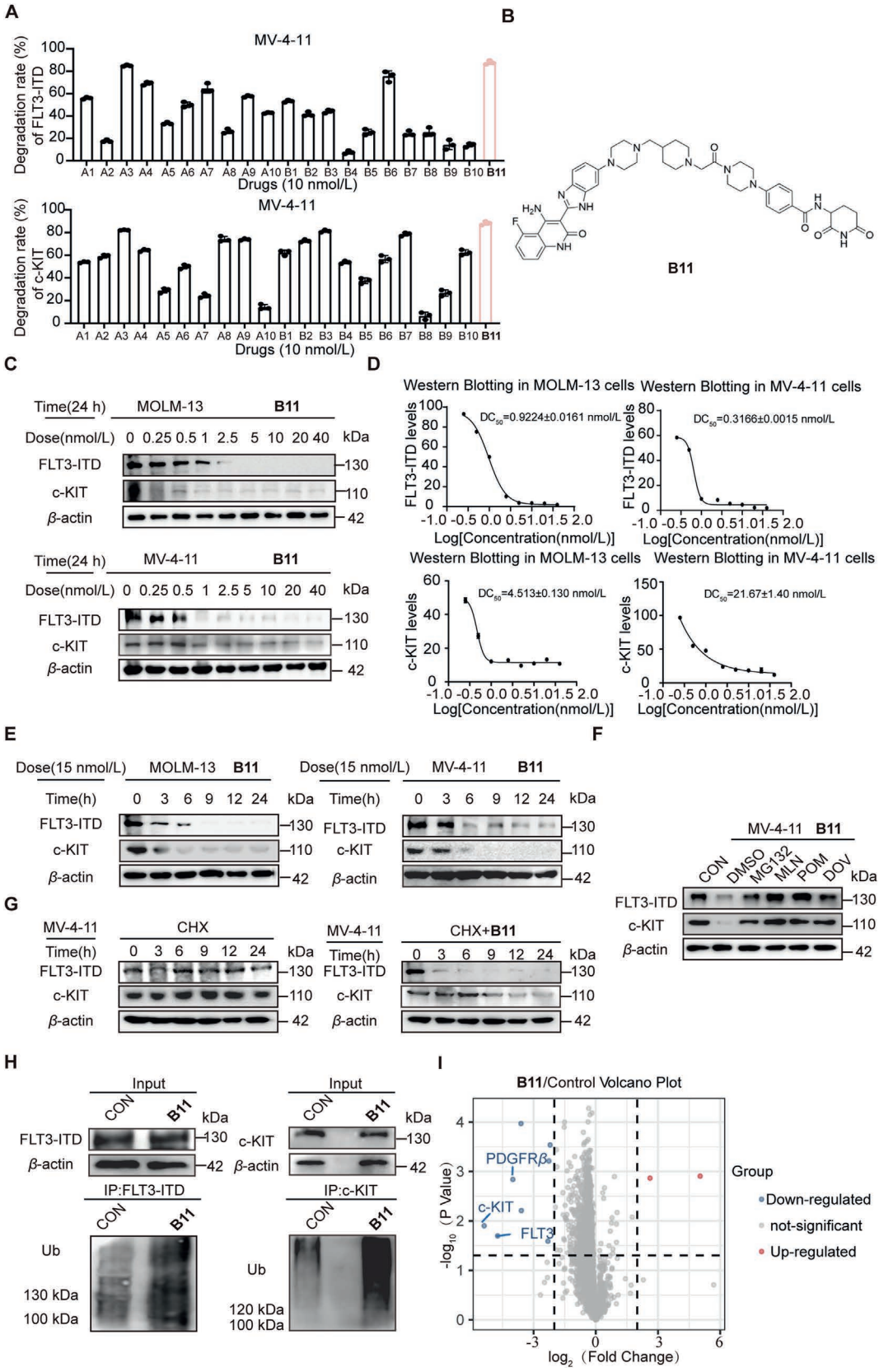

Figure 5 Compound **B11** selectively induced FLT3-ITD and c-KIT degradation through the ubiquitin−proteasome system. (A) Results of screening by Western blot experiments. (B) Chemical structure of **B11**. (C, D) Compound **B11** significantly degraded the FLT3-ITD and c-KIT protein in MOLM-13 and MV-4-11 cells in a concentration-dependent manner. (E) Compound **B11** treatment at the indicated concentration for different times could significantly degrade the FLT3-ITD and c-KIT protein in MOLM-13 and MV-4-11 cells. (F) Before being administrated with

After successfully identifying the degrader molecule **B11**, the pharmacodynamic evaluations in AML cells of this candidate were conducted. Firstly, cell proliferation assay results suggested that **B11** exerted excellent cytotoxic effects on FLT3-ITD$^+$ AML and Ba/F3-FLT3-ITD cell lines, with effects even stronger than Gilteritinib (Fig. 6A and Supporting Information Fig. S10). Cell cycle analysis further revealed that B11 significantly arrested the cell cycle at the G1/S phase (Fig. 6B and Supporting Information Fig. S11A). Meanwhile, both Gilteritinib and **B11** treatment could dose-dependently induce apoptosis in AML cells (Fig. 6C and Fig. S11B). Western blot analysis was performed to assess apoptosis biomarker expression. The results indicated that treatment with both **B11** and Gilteritinib significantly upregulated the expression of cleaved-PARP and cleaved-Caspase 3. Conversely, it was also found that both of the molecules treatment decreased the levels of anti-apoptotic proteins BCL-2 and MCL-1 in a concentration-dependent manner (Fig. 6D). Notably, compared to the Gilteritinib group, **B11** administration could not only completely inhibit the phosphorylation of FLT3-ITD, STAT3, STAT5, and AKT, but also distinctly attenuate the phosphorylation levels of c-KIT and ERK (Fig. 6E). These results were consistent with the previous mechanistic findings and verified the effectiveness of the proposed targeted intervention strategy. Next, we comprehensively evaluated the effects of **B11** and Gilteritinib on the clearance of leukemia stem cells (LSCs). Soft agar colony formation assays also demonstrated that **B11** could significantly suppress the self-renewal ability of LSCs (Fig. 6F and Supporting Information Fig. S12). Differently, Giemsa staining experiments illuminated that, compared to the vehicle and Gilteritinib groups, **B11** treatment could effectively induce a distinct differentiative phenotype in both AML cell lines, as indicated by nuclear segmentation (Fig. 6G). CD11b is a promising biomarker of AML cells differentiation. Consistently, compared to the vehicle and Gilteritinib groups, **B11** incubating could remarkably increase the expression of CD11b in two AML cell lines (Fig. 6H and Supporting Information Fig. S13A). We also collected primary blood samples from relapsed AML patients, including those who relapsed after Gilteritinib treatment. Excitingly, *in vitro* treatment with **B11** could induce significant differentiation in these primary AML cells (Fig. 6I and Fig. S13B).

Armed with these promising *in vitro* results, the *in vivo* models were established to evaluate the anti-AML efficacy of **B11**. To begin with, in the subcutaneous MV-4-11 xenograft model, it was demonstrated that treatment with Gilteritinib and **B11** significantly inhibited AML cell proliferation (Supporting Information Fig. S14A−S14D) and effectively alleviated splenomegaly (Fig. S14E). The experimental animals were sacrificed, and the tumor tissue was collected for Western blot analysis. The results confirmed that **B11** could significantly degrade FLT3-ITD and c-KIT *in vivo* (Fig. S14F). Notably, **B11**-mediated degradation of both proteins occurred rapidly (significant protein degradation was observed within 6 h) and persisted for an extended period (POIs expression resumed in 72 h after drug withdrawal) (Fig. 7A). Furthermore, we developed a tail-vein xenograft model using luciferase-labeled MV-4-11 cell lines (Fig. 7B). Seven days post-injection, *in vivo* imaging confirmed the successful establishment of the AML model. Gilteritinib and **B11** were administered on Day 7. On Day 28, *in-vivo* imaging illustrated that the mice in both the Gilteritinib and **B11** groups achieved hematological complete remission (CR, Fig. S14G). After treatment discontinuation, the survival of the experimental mice was monitored. In the Gilteritinib group, all test animals relapsed and died around Day 48. In contrast, only a few mice in the **B11** group experienced AML relapse, with the majority showing a significantly extended lifespan (Fig. 7C and Fig. S14G). Additionally, the weight of the mice was not affected by the drug (Fig. S14H), and the splenomegaly in the treatment groups were significantly alleviated (Fig. S14I). Notably, unlike the Gilteritinib-treated group, treatment with **B11** significantly induced the expression of the AML differentiation marker CD11b (Fig. 7D and Supporting Information Fig. S15A). Flow cytometric analyzing the peripheral blood, spleen, and bone marrow of the experimental animals demonstrated that the **B11**-treated mice possessing the lowest population of CD45$^+$ cells, indicating these mice maintained hematological complete response (CR) for the longest period (Fig. 7E and Fig. S15B). Moreover, a patient-derived xenograft (PDX) experiment was conducted using primary AML cells from Gilteritinib-resistant patients (Fig. 7F). The results revealed that, compared to the control group, both the Gilteritinib monotherapy group and the Gilteritinib plus Imatinib combination therapy group, the **B11** administration demonstrated excellent therapeutic effects and nearly doubled the overall survival of the experimental mice (Fig. 7G). Additionally, **B11** treatment alleviated splenomegaly (Supporting Information Fig. S16) and notably induced the differentiation of LSCs in the bone marrow and spleen of the mice (Fig. 7H and I and Supporting Information Fig. S17A and S17B). Collectively, treatment of **B11** could effectively suppress the proliferation and stemness of FLT3-ITD $^+$ AML *in vivo* and subsequently extend the overall survival of experimental animals. This compound holds great promise as a potential candidate and offers a novel solution for the targeted treatment of FLT3-ITD$^+$ AML (see Fig. 8).

3. Discussion

FLT3-ITD has emerged as a highly promising therapeutic target for acute myeloid leukemia (AML)[55]. In the past few decades, biopharmaceutical companies have exerted substantial efforts to develop selective and potent FLT3-ITD kinase inhibitors for clinical use. So far, five such inhibitors have been approved by the FDA[56]. Although these drugs can swiftly eliminate AML cells in the peripheral blood, they fail to completely eliminate minimal residual disease (MRD) in the bone marrow[8-12]. Clinical treatments with FLT3 inhibitors, like Gilteritinib, invariably lead to drug resistance and disease relapse[13]. Consequently, exploring the mechanisms underlying drug resistance and disease relapse related

20 nmol/L compound **B11** for 6 h, MV-4-11 cells were pretreated with DMSO, MG132 (1 μmol/L), MLN4924 (1 μmol/L), pomalidomide (1 μmol/L), and dovitinib (1 μmol/L) for 2 h. The FLT3-ITD and c-KIT protein was determined by performing the Western blotting assay. (G) Immunoblot assay of FLT3-ITD and c-KIT protein levels in MV-4-11 cells under cycloheximide (CHX) and compound **B11** exposure. (H) MV-4-11 cells were treated with 20 nmol/L compound **B11** for 4 h. Subsequently, the cells were treated with 2 μmol/L MG132 for 2 h. FLT3-ITD and c-KIT protein was coimmunoprecipitated using an anti-FLT3 antibody and anti-c-KIT antibody. The levels of ubiquitinated protein were assessed through immunoblotting with an anti-ubiquitin antibody. (I) Compound **B11** significantly degraded the FLT3-ITD and c-KIT protein using Proteomics data generated from MV-4-11 cells treated with and without compound **B11**.

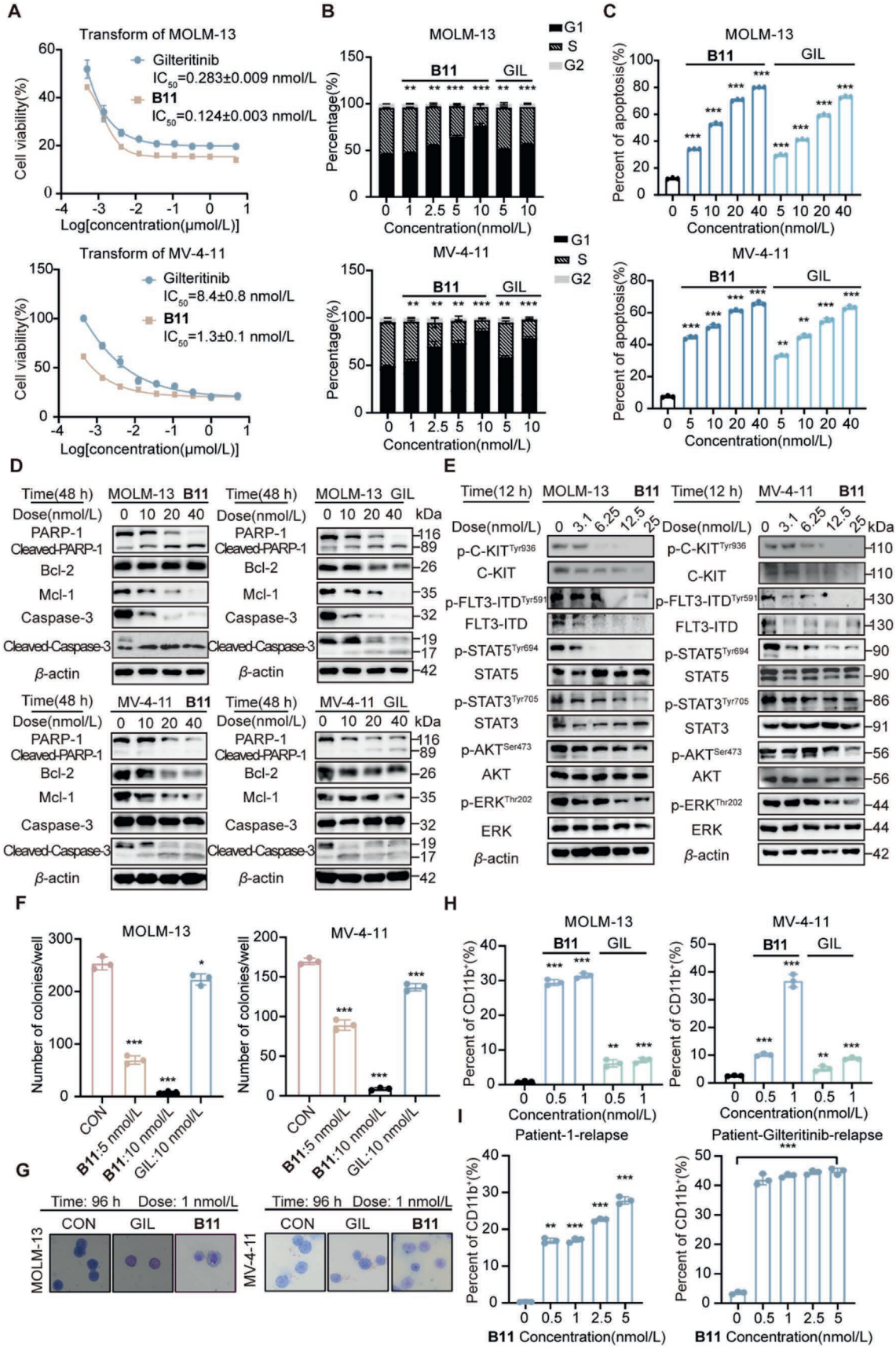

Figure 6 Compound **B11** causes apoptosis and differentiation in AML cells. (A) Proliferation curve of MOLM-13 and MV-4-11 cells under Gilteritinib and compound **B11** or Gilteritinib exposure, respectively, with using CCK-8 assay. (B) Different concentrations of compound **B11**

to Gilteritinib and other FLT3 inhibitors, along with devising innovative targeted solutions, has become a crucial topic in clinical research. Clinical results have demonstrated that simply enhancing the inhibitory potency and selectivity toward FLT3 kinase is insufficient to overcome AML relapse. In-depth investigation and elucidation of the molecular mechanisms underlying the transformation of AML into relapsed and refractory disease following FLT3i-treatment are essential to guide the development of alternative targeted intervention strategies and discovery of novel drug candidate.

In this study, we have explored and identified a novel drug resistance mechanism in FLT3$^+$ AML cells. Through investigations using clinical samples and AML cell lines, we first confirmed that treatment with Gilteritinib could transcriptionally activate c-KIT expression. This serves as the primary mechanism driving the enrichment of c-KIT$^+$ leukemia stem cells (LSCs), thereby inducing drug resistance and recurrence in AML. To investigate the potential mechanisms underlying the transcriptional upregulation of c-KIT, we conducted a metabolomics analysis of these resistant AML cells. The results revealed that Gilteritinib treatment significantly induced lactate metabolic reprogramming in surviving AML cells. Concurrently, transcriptomic data demonstrated distinct upregulation of MCT3 and ACSS2 in these cells, potentiating uptake and utilization lactates in AML cells. We speculate that the mechanism by which Gilteritinib induces an increase in lactate levels mainly comes from two aspects: on the one hand, the endogenous glycolysis pathway in cells, which has been shown in the literature to play an important role in various resistance mechanisms [33]; on the other hand, Gilteritinib upregulates MCT3 expression, promoting the active uptake of exogenous lactate by cells, thereby enhancing AML cells' dependence on lactate metabolism.

MCT3 (monocarboxylate transporter 3), a member of the MCT family, primarily mediates transmembrane transport of monocarboxylic acids such as lactate and pyruvate[34,35]. It is highly expressed in retinal pigment epithelial cells, where it facilitates lactate efflux to maintain retinal energy homeostasis. Notably, previous studies have identified MCT1, MCT2, or MCT4 as highly expressed in drug-resistant cells, contributing to lactate and monocarboxylate transport in the context of cellular metabolic reprogramming[57,58]. However, the role of MCT3 in drug resistance mechanisms of AML cells remains poorly understood. In this study, we found that MCT1, MCT2, and MCT4 expression remained stable in Gilteritinib-resistant AML cells, whereas MCT3 was significantly upregulated. To our knowledge, this is the first report demonstrating a critical role for MCT3 in acquired resistance driven by metabolic reprogramming in AML. Correspondingly, we observed a significant accumulation of lactyl-CoA in the cells. Further lactic acid supplement experiments were further verify these processes. Previous studies have shown that protein lactylation plays a crucial role in regulating protein functions. Notably, histone lactylation at specific lysine residues can potentially alter the chromatin structure at the promoter regions of target genes, thereby promoting gene transcription[39-41]. However, no studies have yet explored the impact of histone lactylation at specific Lysine residues on the transcription of the c-KIT gene. Through ChIP experiments, we identified that the upregulated H3K27la, for the first time, mediated by Gilteritinib treatment stress, could enrich the promoter regions of the c-KIT gene and promote its transcription.

Next, we further uncovered that the positive feedback loop regulatory mechanism contributes to drug resistance and relapse of AML following Gilteritinib treatment. It induced lactate metabolic reprogramming in AML cells. And the resulting H3K27la epigenetic modification could upregulate c-KIT expression and activate its downstream LSCs signaling, thereby conferring drug resistance to AML cells. Concurrently, the epigenetic modification at H3K27la also transcriptionally activated the expression of MCT3 and ACSS2, which further enhanced the uptake and utilization of lactate by drug-resistant cells. This formed a positive feedback regulatory mechanism that further amplifies c-KIT expression.

The results of the aforementioned mechanism study also explained why clinical treatment with c-KIT kinase inhibitors fails to significantly suppress drug resistance and relapse in AML. Sustained upregulation of c-KIT protein led to the infinite amplification of its downstream LCSs signaling, such amplification exceeds the inhibitory capacity of c-KIT inhibitors. Quizartinib is the promising FLT3/c-KIT dual inhibitor. Previous research findings have shown that AML patients treated with Quizartinib still progressed to relapsed and refractory AML. Other c-KIT inhibitors also fail to mitigate AML recurrence[43,44]. These results are consistent with our findings. These implied that c-KIT kinase inhibitors would not fully block the continuously amplified downstream signaling of c-KIT.

To end this, we identified a highly potent and selective FLT3-ITD/c-KIT degrader using the PROTACs technology in order to more effectively disrupt the FLT3-ITD/MCT3/ACSS2/c-KIT positive feedback loop. Compared to Gilteritinib, this degrader could not only notably induce cell death in FLT3-ITD $^+$ AML cells both *in vitro* and *in vivo* but also trigger distinct cell differentiation in drug-resistant LSCs. In CDX and PDX models, compared with the mice in the Gilteritinib treatment and combination treatment with Gilteritinib and Imatinib groups, degrader treatment significantly induced the differentiation of drug-resistant AML cells, minimized relapse rates, and notably improved the

were used to treat MOLM-13 and MV-4-11 cells for 24 h, and cell cycle changes were detected by flow cytometry. The proportion of cells in each phase of the cell cycle was calculated by GraphPad Prism 9 based on three independent repeated experiments. (C) Effect of compound **B11** and Gilteritinib on the apoptosis of FLT3-ITD AML cells. Quantitative analysis of the percentage of apoptotic tumor cells in flow cytometry scatter plot of apoptosis for MOLM-13 and MV-4-11 cells treated with compound **B11** and Gilteritinib for 48 h, respectively. (D) MOLM-13 and MV-4-11 cells were treated with different concentrations of compound **B11** and Gilteritinib for 48 h, cleaved-Caspase-3, cleaved-PARP, MCL-1 and Bcl-2 were detected by Western blot. (E) Immunoblot assay of p-FLT3, p-STAT5, p-AKT, and p-ERK protein levels in MOLM-13 and MV-4-11 cells treated with a concentration gradient of compound **B11** for 12 h. (F) Colony-forming units (CFU) assays for MOLM-13 and MV-4-11 cells administered compound **B11** and Gilteritinib, respectively. (G) Giemsa staining for MOLM-13 and MV-4-11 cells administered compound **B11** and Gilteritinib, respectively. (H) Flow-cytometric analysis of differentiated AML cells with or without compound **B11** and Gilteritinib, respectively. CD11b$^+$ cells were considered differentiated AML cells. (I) Flow-cytometric analysis of differentiated cells of AML patients with or without compound **B11**. Quantitative data were summarized from three independent replicate experiments and expressed as mean $\pm$ SD, $^*P < 0.05$, $^{**}P < 0.01$, $^{***}P < 0.001$ (Student' *t*-test).

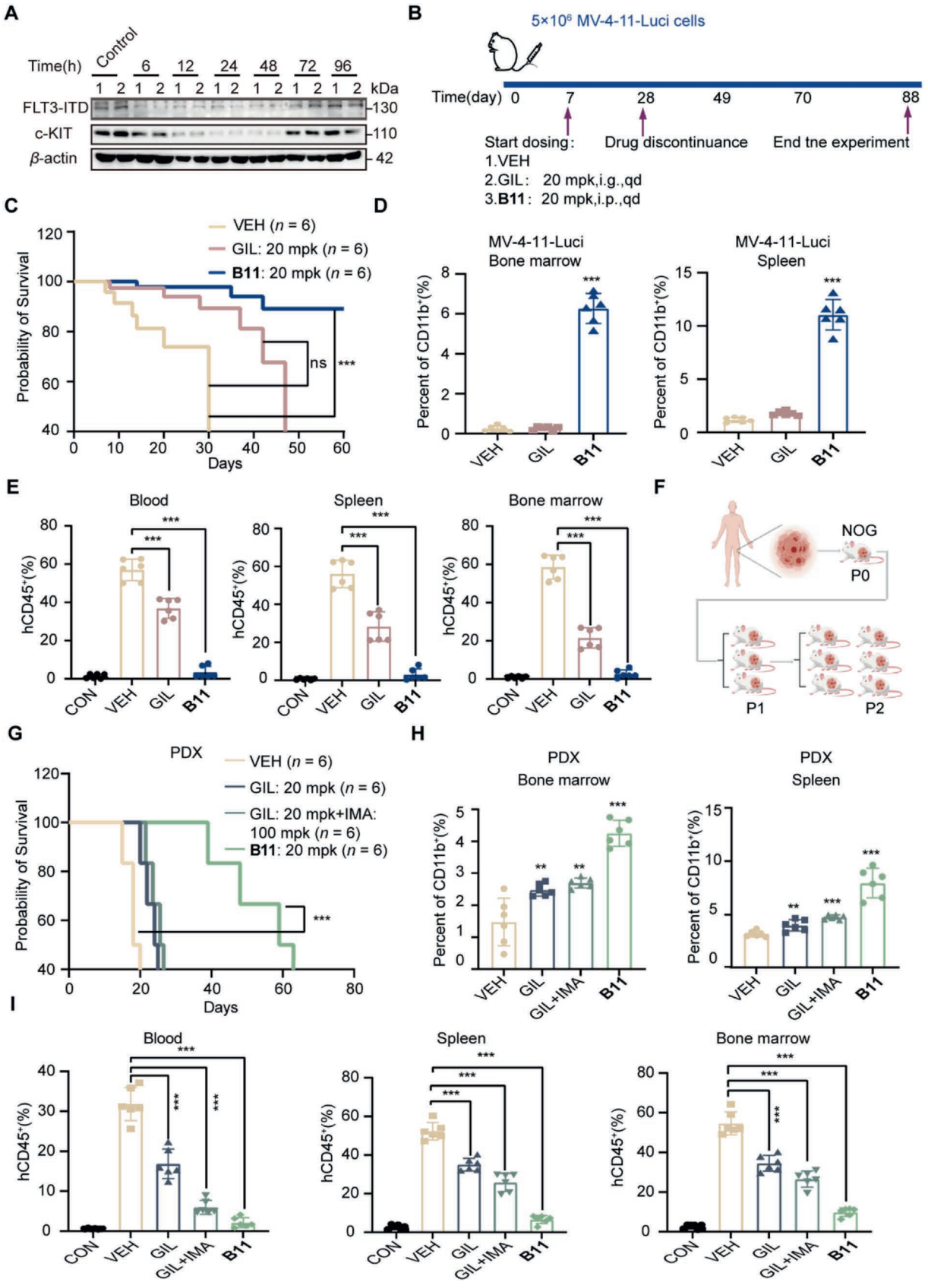

Figure 7 Compound **B11** inhibits the proliferation and metastasis of AML cells *in vivo*. (A) PD experiments: Mice with subcutaneous AML tumors were treated with **B11** (20 mg/kg/day) once the tumors reached a certain size. When the tumor size stabilized, the treatment was stopped. Mice were sacrificed at different time points, and the tumors were collected and ground. Western blotting detected the expression level of

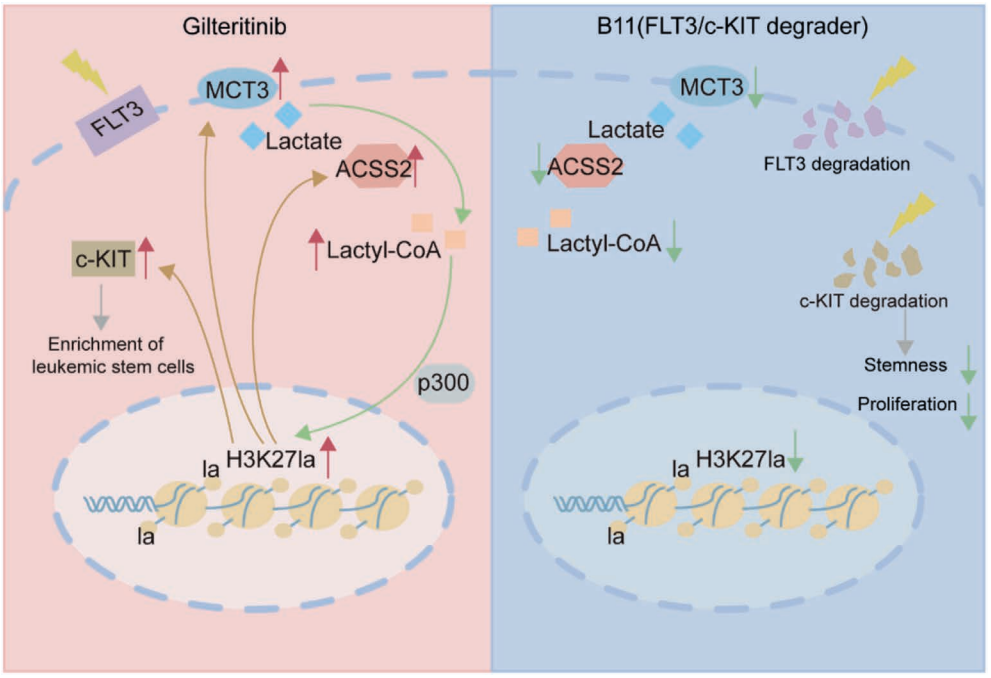

Figure 8 Novel targeted intervention strategy using FLT3-ITD/c-KIT degrader.

overall survival of experimental animals. The PROTAC molecule **B11** has been identified as a candidate drug and is currently undergoing preclinical studies.

Interestingly, when using proteomics to evaluate the selectivity of **B11** for protein degradation, we serendipitously discovered that **B11** also potently degrades PDGFRβ. Previous studies have demonstrated that genetic rearrangements, fusions, and overexpression of PDGFRβ are closely associated with the initiation, progression, and relapse of acute myeloid leukemia (AML). For instance, TEL-PDGFRB and STRN3-PDGFRB gene fusions have been identified as major drivers of AML malignant progression, where the constitutive activation of PDGFRβ kinase domain and downstream signaling pathways promotes AML cell proliferation and chemoresistance[59,60]. Additionally, accumulating evidence indicates that high PDGFRβ expression correlates with poor prognosis and chemoresistance in AML patients. Knockdown of PDGFRβ can inhibit AML cell proliferation, induce apoptosis, and thus hold promise for the treatment of relapsed/refractory AML[61,62]. Furthermore, several studies have highlighted the significant potential of PDGFRβ inhibitors in AML therapy. Literature reports have shown that crenolanib[63], imatinib[64], sunitinib[65], and CT53518[66] can significantly slow leukemia progression by suppressing the kinase activity of PDGFRβ. Collectively, these prior findings suggest that targeting PDGFRβ may benefit AML patients, representing a promising strategy for targeted therapy development.

Despite the promising results of PDGFRβ inhibitors in preclinical studies and small-scale clinical trials, no drugs targeting the inhibition or degradation of PDGFRβ have been approved for AML treatment to date. Future research should focus on conducting large-scale clinical trials to evaluate the efficacy and safety of PDGFRβ inhibition in AML patients with PDGFRβ rearrangements as well as those with relapsed/refractory AML[67].

4. Experimental

4.1. General

All reagents and solvents were purchased from Shanghai Bide Pharmatech Ltd., Co. and MedChemExpress, unless otherwise specified, and used without further purification. Flash column chromatography employed silica gel (100−200 mesh). All compounds were demonstrated to be homogeneous by analytical TLC on precoated silica gel TLC plates (purchased from Qingdao Haiyang Chemical Ltd., Co. 60 F245 on glass, layer thickness 250 μm), and chromatograms were visualized by

FLT3-ITD and c-KIT in tumor samples of mice at different times ($n = 14$). (B−E) MV-4-11 cells were injected into the tail vein of NOG mice. The mice were randomly divided into three groups ($n = 12$) at 7 days after the injection. Compound **B11** (20 mg/kg/day) or Gilteritinib (20 mg/kg/day) was administrated per day for 21 days. On Day 28, dosing is stopped and the mice are observed for death. Diagram (B), Day 28 (the first day of recording survival) stop medication and record survival (C), the number of $CD11b^+$ cells was detected by flow cytometry statistical analysis (D), the number of $CD45^+$ cells was detected by flow cytometry statistical analysis (E) are shown. Data are presented as means ± SEM; $^{***}P < 0.001$, Student's *t*-test. (F−I) *In vivo* assessment for the effect of compound **B11**, Gilteritinib, and Gilteritinib-Imatinib combination on tumor growth in a NOG mouse bearing human AML xenograft tumor. Diagram (F), the survival time of mice (G), the number of CD11b positive cells was detected by flow cytometry statistical analysis (H), the number of CD45 positive cells was detected by flow cytometry statistical analysis (I) are shown. Data are presented as means ± SEM; $^{**}P < 0.01$, $^{***}P < 0.001$, (Student' *t*-test).

phosphomolybdic acid staining. Melting points were determined on a micromelting point apparatus. NMR spectra were recorded in $CDCl_3$ or DMSO-d_6, unless otherwise stated, on Bruker (^{1}H at 400 or 600 MHz, ^{13}C at 100 or 150 MHz) NMR spectrometers, and chemical shifts are reported in units of δ relative to internal TMS. Multiplicities are indicated as br (broadened), s (singlet), d (doublet), t (triplet), q (quartet), and m (multiplet), and coupling constants (J) are reported in hertz (Hz). Low and high-resolution mass spectra were performed in The State Key Laboratory of Medicinal Chemical Biology, College of Pharmacy, Nankai University, Nankai University. Mass spectral data are reported in the form of m/z (intensity relative to base = 100). Synthesis and characterization of all tested compounds are illustrated in the supporting files. Purities of the tested compounds were determined by HPLC analysis using Agela Technologies HPLC using an Agela Technologies MP C18 column (5 μm, 4.6 mm × 50 mm column and methanol/water) and were >95%. Animal tests are all followed ARRIVE guidelines.

4.2. Pharmacokinetics (PK) study

Sprague−Dawley male rats (6−8 weeks old, 220−350 g) were purchased from Academy of Military Medical Sciences (Beijing, China). PK studies were collaborated with Hunan Hengxing Medical Technology Co., Ltd. For a single dose PK study of compound **C3**, 6 rats were divided into different groups: (A) iv of compound **C3** (5 mg/kg), (B) *po* of compound **C3** (25 mg/kg). The drug was dissolved in the 5% DMSO+10% 2-hydroxypropyl-β-cyclodextrin +85% water at pH: 5−6. For PK study, 200 μL blood was collected from different rats at 5, 15, 30, 45 min, 1, 2, 4, 6, 8 and 24 h after treatment. Blood samples were treated with heparin to prevent coagulation. Blood samples were centrifuged for 10 min at 13,000 rpm in a desktop centrifuge to collect plasma. 50 μL plasma samples were combined with 200 μL internal standard (buspirone 100 ng/mL) in MeOH/H_2O (1:1, *v*/*v*), and centrifuged at 15,000 rpm for 10 min at 4 °C. The supernatant (100 μL) was collected and mixed with 5 parts of 50% MeOH/water. Plasma drug concentration was determined by LC−MS/MS.

4.3. Kinetic solubility assay

The kinetic solubility assay was collaborated with the Beijing Ice Bioscience Inc. Prepare test compounds in DMSO at 30 mmol/L. Add 10 μL/vial stock solution into flat bottom glass vials in duplicate in a 96-well rack, followed by adding 990 μL/vial of the assay buffer into the solubility sample plate. Put a PTFE encapsulated stainless steel stick stirrer into each vial, then seal vials using a molded PTDE/SIL silicone plug. Transfer the solubility sample plate to the Thermomixer Comfort plate shaker, 1100 rpm, 25 °C for 2 h. Remove the stir sticks using a big magnet after 2 h' incubation. Transfer the solubility plate sample into the filter plate using Vacuum Manifold. Transfer 10 μL the filtered samples and 10 μL DMSO into 980 μL methanol, further diluted 10-fold in methanol:water (1:1) as filtered samples for LC−MS/MS analysis. Dilute 30 mmol/L test compound stock solutions to 300 μmol/L in DMSO. Transfer 10 μL 300 μmol/L DMSO samples and 10 μL assay buffer into 980 μL methanol, further diluted 10-fold in methanol: water (1:1) as standard samples for LC−MS/MS analysis. Calculate the solubility using Microsoft Excel.

4.4. LC−MS/MS

The samples were dissolved in methanol (solvent A), filtered through a 0.2 μm membrane (Merck Millipore), and analyzed using a homemade C18 reversed-phase column (30 °C) on a UPLC system. Separation was achieved with a linear gradient from 5% to 35% methanol (containing 2 mmol/L ammonium lactate) over 15 min at 0.2 mL/min. For LC−MS/MS detection, 5 μL aliquots were injected into an online system equipped with an electrospray ionization (ESI) source and tandem mass spectrometer. Lactyl-CoA was eluted with 1 mL of 25 mmol/L ammonium lactate in methanol.

4.5. Human liver microsomal stability

The experiments were collaborated with PreceDo Pharmaceuticals Co., Ltd. Hefei, China. The human microsomes were commercially available (BioIVT, X008005). Microsome stability was evaluated by incubating test compound (1 μmol/L final concentration) with 1 mg/mL hepatic microsomes at 37 °C. The reaction was initiated by adding NADPH (1 mmol/L final concentration). The mixtures were vortexed gently at 37 °C. At each time point of 0, 5, 15, 30 and 60 min, an aliquot was removed from each tube. Terfenadine/tolbutamide in ACN/MeOH (1:1, *v*/*v*) was added to quench and precipitate the microsomal incubations. Samples were capped and vigorously vortexed and then centrifuged at 4 °C. An aliquot of each supernatant was transferred for LC−MS/MS analysis. The MS detection was performed using a QTRAP 6500+ Low Mass instrument. Each compound was analyzed by reverse phase HPLC using an XBridge BEH C18 2.5 μm 2.1 mm × 50 mm.

4.6. Molecular modeling

Molecular docking was performed with the crystal structure of FLT3 (PDB ID: 6JQR), c-KIT (PDB ID: 8PQ9) as an input. The three-dimensional structure of molecular was obtained, and its energy was minimized by Chem 3D 22.00. Polar hydrogens and protein preparation were added to proteins with the AutoDock Tools program, and docking studies were performed using AutoDock Vina 1.05.36. Figures were generated using Pymol 3.0 (Educational open source).

4.7. Cell lines and cell culture

Human leukemia cell lines MV-4-11 (ATCC CRL-9591) and MOLM-13 were, respectively, cultured in IMDM or DMEM supplemented with 10% fetal bovine serum (FBS, Biological Industries, 04-001-1A/B), 100 units/mL penicillin G, and 0.1 mg/mL streptomycin (life science, P1400) at 37 °C in the presence of 5% CO_2.

4.8. Cell cytotoxicity assay

CCK-8 assays were used to assess the drug sensitivity of different leukemia cell lines. The cells were seeded in 96-well plates (8.0×10^3 cells per well) for human leukemia cell lines MV-4-11 and MOLM-13 in a final volume of 80 μL. Then, 20 μL of compounds was added at different concentrations. After 72 h of drug incubation, 10 μL of CCK-8 (Vazyme, A311-01) solution was added to each well and incubation was continued for another 3−4 h. Optical density (OD) of formazan concentration was read

at 450 nm with THERMO FISHER Multiskan FC. The concentrations required to inhibit growth by 50% (IC_{50}) were calculated with GraphPad Prism7 as previously described.

4.9. Western blot analysis

MV-4-11 and MOLM-13 (5×10^5 per well) were seeded in six-well culture plates, treated with the compound at indicated concentrations for appropriate time or indicated time for appropriate concentrations and lysed in RIPA lysis buffer supplemented with protease inhibitors cocktail/PMSF and dephosphorylase inhibitor NaF. The protein concentration was measured with the BCA Protein Assay kit (Beyotime Biotechnology, P0012). Equal amounts of proteins were electrophoresed by SDS-PAGE (8%−15%) under denaturing conditions and transferred onto the PDVF membranes (Millipore Corporation, IPVH00010). Membranes were blocked in 5% nonfat milk (BD Difco, 232100) and then incubated with primary antibodies. After being washed, the membranes were incubated with secondary antibodies and detected by a Luminescent Image Analyzer LSA 4000 (GE, Fairfield, CO). Antibodies used in this study were as follows: anti-FLT3 (Proteintech, 21049-1-AP), anti-β-actin (Proteintech, 66009-1-Ig), anti-Phospho-FLT3 (Cell Signaling Technology, 3466S), anti-STAT5 (Cell Signaling Technology, 25656S), anti-Phospho-STAT5 (Cell Signaling Technology, 4322S), anti-Caspase-3 (Cell Signaling Technology, 9662S), anti-cleaved Caspase-3 (Cell Signaling Technology, 9661S), anti-Mcl-1 (Cell Signaling Technology, 94296S), anti-Bcl-2 (Cell Signaling Technology, 15071S), anti-PARP (Santa Cruz Biotechnology, sc-53643), anti-cleaved PARP (Santa Cruz Biotechnology, sc-8007), anti-Phospho-AKT (Santa Cruz Biotechnology, sc-377556), anti-AKT (Santa Cruz Biotechnology, sc-5298), anti-Phospho-ERK (Santa Cruz Biotechnology, sc-136521), anti-ERK (Santa Cruz Biotechnology, sc-271269), anti-STAT3 (Proteintech, 10253-2-AP), anti-Phospho-STAT3 (Cell Signaling Technology, 9145), anti-c-KIT (zenbio, 347321), anti-Phospho-c-KIT (zenbio, 370316), anti-PDGFRβ (Proteintech, 32335-1-AP), anti-MCT1 (Santa Cruz Biotechnology, sc-36550), anti-MCT2 (zenbio, 680408), anti-MCT3 (Affinity, DF13644), anti-MCT4 (Santa Cruz Biotechnology, sc-376465), anti-ACSS2 (Santa Cruz Biotechnology, sc-398559), anti-ubiquitin (Proteintech, 10201-2-AP), anti-Histone-H3 (Proteintech, 17168-1-AP), anti-H3K9la (PTM BIO, PTM-1419RM), anti-H3K18la (PTM BIO, PTM-1415RM), anti-H3K23la (PTM BIO, PTM-1413RM), anti-H3K27la (PTM BIO, PTM-1428), anti-Histone-H4 (zenbio, 344323), anti-H4K5la (PTM BIO, PTM-1407RM), anti-H4K16la (PTM BIO, PTM-1417RM).

4.10. Apoptosis assay

MV-4-11 and MOLM-13 (5×10^5 per well) were plated into six-well culture plates and treated without or with the compound at the indicated concentration for 48 h. The treated cells were then collected and washed twice with cold PBS. Cell apoptosis was detected using an Annexin V-FITC/PI Apoptosis Detection kit (Beyotime, C1063) by a BD flow cytometer.

4.11. Immunoprecipitation assay

MV-4-11 cells were pretreated with compound **B11** for 4 h and then treated with 2 μmol/L MG132 for 2 h. The cells were extracted in RIPA buffer. The lysates were centrifuged at 12,000×*g* for 15 min and incubated at 4 °C for 16 h with 5 μg of FLT3 antibody (Proteintech, 21049-1-AP) and c-KIT antibody (Santa Cruz Biotechnology, sc-393910), respectively. Then, 50 μL of protein A/G agarose (Santa Cruz Biotechnology, sc-2003) was added and incubated at 4 °C for 8 h. Protein A/G agarose was then recovered by centrifugation at 1000×*g*, washed six times with wash buffer (*n* 50 mmol/L Tris−HCl (pH 8.0), 150 mmol/L NaCl, 0.1% (*v*/*v*) NP-40), resuspended in 50 μL of 2 × SDS loading buffer, boiled at 99 °C for 10 min, and centrifuged at 12,000×*g* for 10 min. The supernatant was then analyzed by SDS-PAGE, followed by Western blotting using an anti-ubiquitin antibody.

4.12. RNA extraction and qRT-PCR

MV-4-11 and MOLM-13 cells were cultured in six-well plates (5×10^5 per well) for 24 h, followed by treatment with compound Gilteritinib for 24 h. The residue cells were harvested with Trizol reagent (Invitrogen, Frederick, MD, USA). First-strand cDNA was generated using the HiScript II Reverse Transcriptase (Vazyme, R223-01). qRT-PCR was performed in the Lightcycler 96 Real-Time PCR System (Roche) using AceQ qPCR SYBR Green Master Mix (Vazyme, Q111).

The mRNA expression of c-KIT, MCT3, ACSS2 and β-actin was determined by qRT-PCR. Primers used for qRT-PCR:

c-KIT,
forward 5′-CACCGAAGGAGGCACTTACACA-3′,
reverse 5′- TGCCATTCACGAGCCTGTCGTA-3′
MCT1,
forward 5′-TTGTTGGTGGCTGCTTGTCAGG-3′,
reverse 5′-TCATGGTCAGAGCTGGATTCAAG-3′
MCT2,
forward 5′- TGCTGGCTGTTATGTACGCAGG-3′,
reverse 5′- GCCAACACCATTCCAAGACAGC-3′
MCT3,
forward 5′-TGCAGTTCGAGGTGCTCATGGC-3′,
reverse 5′-GTTCTTCAACACATCCACCAGGC-3′
MCT4,
forward 5′-GCCATCTTTGCTGGTGGTTACC-3′,
reverse 5′-TGGTCCAGAAAGGACAGCCATC-3′.
ACSS2,
forward 5′-GGTGACCAAGTTCTACACAGCAC-3′,
reverse 5′-GTTCACCCACTGTGCCTAACAC-3′
β-Actin,
forward 5′-CACCATTGGCAATGAGCGGTTC-3′,
reverse 5′-AGGTCTTTGCGGATGTCCACGT-3′

4.13. RNA sequencing

The RNA sequencing was performed by OEbiotech (Shanghai, China). Briefly, the collected cells were processed for RNA isolation using TRIzol reagent (Invitrogen) according to manufacturer's protocol. To the constructed RNA library, remove the rRNA using the TruSeq Stranded Total RNA with Ribo-Zero Gold kit, and reverse transcription was performed for cDNA. The purified DNA was amplified by PCR. followed by qualified inspection with Agilent Bioanalyzer 2100 system (Agilent Technologies, USA), and then Illumina sequencer was used for sequencing. The differentially expressed mRNA were further analyzed based on $|\text{Fold Change}| > 1.5$ and P value < 0.05. The Database for Annotation, Visualization and Integrated Discovery (DAVID, https://david.ncifcrf.gov/) was used to perform Gene Ontology (GO) functional and KEGG pathway enrichment analyses, considered $P < 0.05$ as statistically significant. RNA-seq data are shown in Supporting Information

4.14. Untargeted metabolomics

Thank Repugene Technology (Hangzhou, China) for performing the experiment and analysis of untargeted metabolomics. We will perform an untargeted metabolomic analysis of MOLM-13 cells treated with and without 25 nmol/L Gilteritinib. Cell collection: Centrifuge at 300×*g*, 4 °C for 5 min, discard the supernatant medium, collect in a 2 ml EP tube, then wash cells twice with 1 × PBS. After each wash, obtain cell pellets by centrifugation (300×*g*, 4 °C for 5 min). Place at −80 °C for 15 min to fully deactivate enzymes. If not extracted immediately, it can be stored in a −80 °C freezer; Cell lysis and metabolite extraction: Add 200 μL of 80% methanol solution (containing a mixture of internal standards), use an ultrasonic cell disruptor to lyse cells, then add 800 μL of 80% methanol solution (containing a mixture of internal standards), vortex for 1 min; Centrifuge at 14,000×*g*, 4 °C for 10 min, transfer the supernatant to a new 2 mL centrifuge tube; PQC preparation: Mix an equal amount of supernatant from each sample in step (3) to create a PQC sample; After vacuum freeze-drying, resuspend in 100 μL of 10% methanol/90% water solution, vortex for 30 s, sonicate for 1 min, centrifuge at 14,000×*g*, 4 °C for 10 min, transfer the supernatant to a sample vial for mass spectrometry analysis.

4.15. Lactyl-CoA analysis

After drug treatment of MV-4-11 and MOLM-13 in 5 × 10^5 per well, they were collected and washed with PBS that had been cooled in advance, 2000 rpm, 5 min, and centrifugation. After resuspension of cells using pre-chilled 80% methanol (methanol/water, 4:1), sonication. After ultrasonic, centrifuge at 13,000 rpm for 10 min, and centrifuge to take the supernatant. The supernatant was filtrated through a 0.22 μmol/L filter and then detected by LC−MS/MS.

4.16. Lactic acid content assay

About 1 × 10^4 AML cells were collected and measured by the lactic acid production using the Lactic Acid Content (LA) Assay Kit according to the manufacturer's instructions.

4.17. ChIP-qPCR

Select a 15 cm cell culture dish, MV-4-11 with a growth density of 80%, and MOLM-13 cells for experiments, add 37% formaldehyde to the ultra-clean bench to make its final concentration of 1% and mix well to ensure that the cells can be fully in contact with formaldehyde. After fixation at room temperature for 10 min, 1 mL of pre-prepared 2 mol/L glycine was added, and the fixation was terminated and discarded. After washing the cells twice with PBS, add 10 mL of ChIP SDS buffer. Centrifuge at room temperature at 1200 rpm for 6 min, discard the supernatant, resuspend the cells with 1 mL of immunoprecipitation (IP) buffer, and perform ultrasound to interrupt the chromatin in the cells. The fragment size needs to be around 500 bp after ultrasound. Centrifuge the ultrasonic sample at 12,000 rpm for 5 min. The supernatant was then transferred to a 1.5 mL EP tube, 1/50 of the experimental input group was pipetted and placed at 4 °C, and the remaining fraction was divided into 2 groups, one was added with 1 μg of the corresponding experimental antibody as the IP group, and the other was added with 1 μg of IgG antibody as the IgG group. Incubate overnight at 4 °C on a runner. On the second day, 40 μL of Protein A/G immunoprecipitation magnetic beads were added to each of the two groups for 4 h, and the crosslinking buffer was added to the solution crosslinking buffer at 65 °C overnight for product purification, and then the samples were diluted separately and used as a template for RT-qPCR experiments.

c-KIT Promoter sequence,
Primer 1, forward 5′-ATTGTGAGGGCTTTCCTGTG-3′,
reverse 5′-CCAGAGAATCCGAACACTCC-3′
primer 2, forward 5′-GCTGAAGGTGCTGAGAAGGT-3′,
reverse 5′-CAGGGTGAAGAGGGAAGTGT-3′
ACSS2 Promoter sequence,
Primer 1, forward 5′-CACCCTCTCCCTTGTCACAC-3′,
reverse 5′-CTGTCCTTGCCAACCTCGAT-3′
primer 2, forward 5′-GAGCTGGTGAAGGTGCTGAT-3′
reverse 5′-CAGGTGAAGAGGGAAGTGTC-3′
MCT3 Promoter sequence,
Primer 1, forward 5′-CCAACACATGCCCTCTCTGT-3′,
reverse 5′-CTTATTTGGGGGACAGGGCA-3′
primer 2, forward 5′-GTGCTGAAGGTGCTGAGAAG-3′,
reverse 5′-AGGGTGAAGAGGGAAGTGTG-3′

4.18. Flow cytometric analysis

The antibodies targeting following proteins were purchased from Biolegend: FITC anti-human CD11b Antibody (#301329). MV-4-11 and MOLM-13 (5 × 10^5 per well) were plated into 6-well culture plates and treated without or with compound at indicated concentration for 96 h. The treated cells were then collected and washed twice with cold PBS. The cells were resuspended in 100 μL PBS. The cells can be pre-incubated with 5 μL of Human TruStain FcX™ (BioLegend, 422301) per 100 μL of cell suspension for 5−10 min at room temperature. Then, add 5 μL antibodies and incubate on ice for 15−20 min in the dark. Wash cells twice with 2 mL of PBS by centrifugation at 350×*g* for 5 min. Analyzed using a BD flow cytometer. Data analysis was performed using FlowJo software.

4.19. Giemsa staining

Wright-Giemsa staining kit was from Beyotime (#C0131). Briefly, the cytospin slides were prepared. Wright-Giemsa staining was carried out, following standard instructions.

4.20. Colony formation

Colony formation was assessed using a soft agar assay. Cells were suspended in IMDM, DMEM containing 0.6% agarose and 20% fetal bovine serum and plated on top of a solidified layer of IMDM, and DMEM containing 1.2% agarose and 20% fetal bovine serum without or with compound. The cells were plated at a density of 1000 cells/well in 60 mm plates and cultured at 37 °C in the presence of 5% CO_2. After 20−30 days of growth, colonies of >50 cells were scored.

4.21. siRNA transfection

Cells were transfected with siRNAs using Lipofectamine® RNAiMAX transfection reagent (Thermo Fisher Scientific, Invitrogen, 13778075) following the manufacturer's protocol and analyzed 72 h later. siRNA knockdown efficiencies were validated

by western blotting. The sequences of the siRNAs used were as follows:

si-c-KIT-1: 5′-ACTTCATCTAACGAGATTAAA-3′;
si-c-KIT-2: 5′-GCGACGAGATTAGGCTGTTAT-3′;
Vector: pLenti-U6-CBH-TurboGFP-P2A-Puro-ncshRNA
si-ACSS2-1: 5′-GCTTCTGTTCTGGGTCTGAAT-3′;
si-ACSS2-2: 5′-CGGTTCTGCTACTTTCCCATT-3′; Vector: pLKO.1-copGFP-PURO.

4.22. Lentivirus infection

Overexpression of genes was performed by lentivirus transduction. pCDH-EF1-MCS-CMV-copGFP-T2A-Puro overexpression vector constructs were from Synbio Technologies (Suzhou, China). The codon optimized nucleotide sequences were chemically synthesized. For ACSS2 overexpression experiments, we used such vector. The sequences of primers were listed in Supporting Information Table S5. Lentiviral vector constructs were transfected with packaging and envelope plasmids to 293 FT cells. Viral supernatant was harvested at 72 h after transfection, filtered through a 0.45 μm filter, and then added to the cultured cells in the media supplemented with 1 mg/mL PEI MW40000 (Yeasen, 40816ES03) according to the instruction manual. Twenty-four hours after infection, the virus-containing media were removed and replaced with fresh media. The transfected cells were selected by FACS or puromycin at 0.2 mg/mL for stable cell line establishment.

4.23. Animal study

All animal experiments were performed in accordance with the guidelines of the Institutional Animal Care and Use Committee (IACUC) and approved by the Laboratory Animal Ethics Committee of Nankai University (No. 2024-SYDDLL-000078). All efforts were made to minimize animal suffering and reduce the number of animals used.

For the mouse subcutaneous xenograft model using a leukemia cell line, MV-4-11 cells (5×10^6 cells/mouse) were inoculated into the subcutaneous of Balb/c nude mice. Compound **B11** group (20 mg/kg/day, $n = 12$), Gilteritinib group (20 mg/kg/day, $n = 12$), and control group ($n = 12$) were orally administered for 16 days.

For mouse orthotopic transplantation models using leukemia cell lines, MV-4-11 cells (5×10^6 cells/mouse) were inoculated into the tail vein of NOG mice, which were pretreated with cyclophosphamide (150 mg/kg) for 2 days before injection for immunosuppression. The mice were divided into three groups ($n = 12$) at 7 days after the injection. Compound **B11** (20 mg/kg/day) or Gilteritinib (20 mg/kg/day) was orally administrated for 21 days. On the 28th day, treatment was terminated and the mice ($n = 6$) are observed for death. Finally, bone marrow (BM) cells were collected. The percentage of human CD45-positive viable cells among the BM cells was measured by BD flow cytometry after staining with an anti-human CD45 antibody (Invitrogen, 11-0459-42). Human CD45-positive cells were defined as residual leukemia in the BM of femurs. 300The remaining mice ($n = 6$) in each group were utilized for the analysis of survival period.

4.24. Pharmacodynamic (PD) study

The experiment selected 14 BALB/c nude mice to establish an MV-4-11 subcutaneous tumor model, simulating the AML tumor growth environment. The mice were divided into two groups: 2 as the control group without treatment, and the remaining 12 as the experimental group, which received daily **B11** (20 mg/kg/day). After the tumor size stabilized, treatment was stopped, and at 6, 12, up to 96 h post-withdrawal, 2 mice from the experimental group were sacrificed at each time point, and tumor tissues were collected and stored at −80 °C. Subsequently, the tumor tissues were ground, proteins extracted, and the expression of FLT3-ITD and c-KIT proteins was assessed.

4.25. Generation and analysis of patient-derived xenografts (PDX) model

PDX experiments were approved by Ethics Committee of Shenzhen University General Hospital (No. KYLL-20230802A).

$CD34^+$ cells from FLT3-ITD^+ AML patients were enriched and then were transplanted (5×10^5 cells per mouse) into sub-lethally irradiated NOG female mice (T001475, GemPharma tech, Jiangsu, China) *via* the tail vein. Experimental animals were randomly divided into three groups ($n = 12$ each), namely the Vehicle group, the Compound **B11** group (20 mg/kg/day) and the Gilteritinib group (20 mg/kg/day). On the 20th day, spleens and bone marrows were harvested from mice ($n = 6$) in each group to detect $CD11b^+$ by flow cytometry. The remaining ($n = 6$) in each group were subjected to survival analysis.

4.26. Statistical analysis

All statistical analyses were conducted using GraphPad Prism 9.0 software. Statistically significant differences were determined by Student's *t*-test, and *P* values less than 0.05 were considered statistically significant in all cases.

Acknowledgments

This work was supported by the National Natural Science Foundation of China (82470167, 824B2114, 82373134, 82574434, 82404442 and 82270172), the International Science and Technology Cooperation Project of China (2022YFE0133300), the Fundamental Research Funds for the Central Universities, (735-63253255, China), China Postdoctoral Science Foundation (No. 2024M751531), Tianjin Natural Science Foundation (24JCYBJC01990, 25JCZDJC00170, China) and the Science and Technology Development Fund of Tianjin Education Commission for Higher Education (No. 2025ZD011, China). Shenzhen Science and Technology Program (No. RCYX20221008092851074, RCBS20210706092216031 and JCYJ20220531103014031, China), Shenzhen Medical Research Fund (No. A2303007, China), Shenzhen University 2035 Initiative (No. 2023C006, China). Scientific Instrument and Technology R&D Project of Nankai University (Grant No. 24NKSYJS09, China).

Author contributions

Ms Yanli Zhao conducted the exploration of molecular mechanisms, screening of drug molecules, and pharmacodynamic evaluation. Mrs Yubo Wang designed, synthesized, and characterized all PROTAC molecules. Ms Ning Liu performed the analysis of protein mass spectrometry. Ms Qi Hao assisted in completing the biological evaluation. Ms Yijie Yang and Ms Jialu Li assisted in the synthesis and characterization of compounds. Dr. Ziqi Huang and Dr. Lan Ma proofread the biological data and created the

figures. Prof. Dr. Shuang Yang participated in the design of the project, provided financial support, and offered supervision. Dr. Shuangwei Liu participated in the project design and proofread the data related to compound synthesis. Prof. Dr. Jingfeng Zhou, as a clinical expert, participated in the project design, provided patient samples, and conducted PDX experiments. Prof. Dr. Guang Yang, the project leader and initiator, designed the project, provided financial support, supervised the project, and drafted the manuscript. All authors have given approval to the final version of the manuscript.

Conflicts of interest

All other authors have no competing interests.

Supporting information

Supporting information to this article can be found online at https://doi.org/10.1016/j.apsb.2026.01.045.

References

1. DiNardo CD, Cortes JE. Mutations in AML: prognostic and therapeutic implications. *Hematology Am Soc Hematol Educ Program* 2016;**1**:348−55.
2. Khwaja A, Bjorkholm M, Gale RE, Levine RL, Jordan CT, Ehninger G, et al. Acute myeloid leukaemia. *Nat Rev Dis Primers* 2016;**2**:16010.
3. Snaith O, Poveda-Rogers C, Laczko D, Yang G, Morrissette JJD. Cytogenetics and genomics of acute myeloid leukemia. *Best Pract Res Clin Haematol* 2024;**37**:101533.
4. Daver N, Schlenk RF, Russell NH, Levis MJ. Targeting FLT3 mutations in AML: review of current knowledge and evidence. *Leukemia* 2019;**33**:299−312.
5. Kantarjian H, Borthakur G, Daver N, DiNardo CD, Issa G, Jabbour E, et al. Current status and research directions in acute myeloid leukemia. *Blood Cancer J* 2024;**14**:163.
6. Lagunas-Rangel FA, Chávez-Valencia V. FLT3-ITD and its current role in acute myeloid leukaemia. *Med Oncol* 2017;**34**:114.
7. Dhillon S. Gilteritinib: first global approval. *Drugs* 2019;**79**:331−9.
8. Ghiaur G, Levis M. Mechanisms of resistance to FLT3 inhibitors and the role of the bone marrow microenvironment. *Hematol Oncol Clin N Am* 2017;**31**:681−92.
9. Antar AI, Otrock ZK, Jabbour E, Mohty M, Bazarbachi A. FLT3 inhibitors in acute myeloid leukemia: ten frequently asked questions. *Leukemia* 2020;**34**:682−96.
10. Joshi SK, Nechiporuk T, Bottomly D, Piehowski PD, Reisz JA, Pittsenbarger J, et al. The AML microenvironment catalyzes a stepwise evolution to gilteritinib resistance. *Cancer Cell* 2021;**39**: 999−1014.
11. Gui P, Bivona TG. Stepwise evolution of therapy resistance in AML. *Cancer Cell* 2021;**39**:904−6.
12. Tefferi A, Nicolosi M, Penna D, Vallapureddy R, Hanson CA, Pardanani A, et al. Cytogenetic clonal evolution in myeloproliferative neoplasms: contexts and prognostic impact among 648 patients with serial bone marrow biopsies. *Leukemia* 2019;**33**:2522−53.
13. Short NJ, Konopleva M, Kadia TM, Borthakur G, Ravandi F, DiNardo CD, et al. Advances in the treatment of acute myeloid leukemia: new drugs and new challenges. *Cancer Discov* 2020;**10**: 506−25.
14. Abbas HA, Alfayez M, Kadia T, Ravandi-Kashani F, Daver N. Midostaurin in acute myeloid leukemia: an evidence-based review and patient selection. *Cancer Manag Res* 2019;**11**:8817−28.
15. Thomas CM, Campbell P. FLT3 inhibitors in acute myeloid leukemia: current and future. *J Oncol Pharm Pract* 2019;**25**:163−71.
16. Zhao J, Song Y, Liu D. Gilteritinib: a novel FLT3 inhibitor for acute myeloid leukemia. *Biomark Res* 2019;**7**:19.
17. Pulte ED, Norsworthy KJ, Wang Y, Xu Q, Qosa H, Gudi R, et al. FDA approval summary: gilteritinib for relapsed or refractory acute myeloid leukemia with a FLT3 mutation. *Clin Cancer Res* 2021;**27**:3515−21.
18. Perl AE, Hosono N, Montesinos P, Podoltsev N, Martinelli G, Panoskaltsis N, et al. Clinical outcomes in patients with relapsed/refractory FLT3-mutated acute myeloid leukemia treated with gilteritinib who received prior midostaurin or sorafenib. *Blood Cancer J* 2022;**12**:84.
19. Shi W, Jin W, Xia L, Hu Y. Novel agents targeting leukemia cells and immune microenvironment for prevention and treatment of relapse of acute myeloid leukemia after allogeneic hematopoietic stem cell transplantation. *Acta Pharm Sin B* 2020;**10**:2125−39.
20. Patel RK, Weir MC, Shen K, Snyder D, Cooper VS, Smithgall TE. Expression of myeloid Src-family kinases is associated with poor prognosis in AML and influences Flt3-ITD kinase inhibitor acquired resistance. *PLoS One* 2019;**14**:e0225887.
21. Weis TM, Marini BL, Bixby DL, Perissinotti AJ. Clinical considerations for the use of FLT3 inhibitors in acute myeloid leukemia. *Crit Rev Oncol Hematol* 2019;**141**:125−38.
22. McMahon CM, Ferng T, Canaani J, Wang ES, Morrissette JJD, Eastburn DJ, et al. Clonal selection with RAS pathway activation mediates secondary clinical resistance to selective FLT3 inhibition in acute myeloid leukemia. *Cancer Discov* 2019;**9**:1050−63.
23. Perl AE, Martinelli G, Cortes JE, Neubauer A, Berman E, Paolini S, et al. Gilteritinib or chemotherapy for relapsed or refractory FLT3-mutated AML. *N Engl J Med* 2019;**381**:1728−40.
24. Li G, Yao J, Lu Z, Yu L, Chen Q, Ding L, et al. Simvastatin preferentially targets FLT3/ITD acute myeloid leukemia by inhibiting MEK/ERK and p38-MAPK signaling pathways. *Drugs R D* 2023;**23**: 439−51.
25. Rabik CA, Wang J, Pratilas CA. FLT3-IRAK dual targeting: an exciting new therapeutic option guided by adaptive activation of immune response pathways. *Ann Transl Med* 2020;**8**:511.
26. Damnernsawad A, Bottomly D, Kurtz SE, Eide CA, McWeeney SK, Tyner JW, et al. Genome-wide CRISPR screen identifies regulators of MAPK and MTOR pathways mediating sorafenib resistance in acute myeloid leukemia. *Haematologica* 2022;**107**:77−85.
27. Russkamp NF, Myburgh R, Kiefer JD, Neri D, Manz MG. Anti-CD117 immunotherapy to eliminate hematopoietic and leukemia stem cells. *Exp Hematol* 2021;**95**:31−45.
28. Xu X, Yu Y, Zhang W, Ma W, He C, Qiu G, et al. SHP-1 inhibition targets leukaemia stem cells to restore immunosurveillance and enhance chemosensitivity by metabolic reprogramming. *Nat Cell Biol* 2024;**26**:464−77.
29. Eisenwort G, Sadovnik I, Keller A, Ivanov D, Peter B, Berger D, et al. Phenotypic characterization of leukemia-initiating stem cells in chronic myelomonocytic leukemia. *Leukemia* 2021;**35**:3176−87.
30. Chu Y, Chen Y, Li M, Shi D, Wang B, Lian Y, et al. Six1 regulates leukemia stem cell maintenance in acute myeloid leukemia. *Cancer Sci* 2019;**110**:2200−10.
31. Somervaille TC, Cleary ML. Identification and characterization of leukemia stem cells in murine MLL-AF9 acute myeloid leukemia. *Cancer Cell* 2006;**10**:257−68.
32. Joshi SK, Nechiporuk T, Bottomly D, Piehowski PD, Reisz JA, Pittsenbarger J, et al. The AML microenvironment catalyzes a stepwise evolution to gilteritinib resistance. *Cancer Cell* 2021;**39**: 999−1014.e8.
33. Zavorka Thomas ME, Lu X, Talebi Z, Jeon JY, Buelow DR, Gibson AA, et al. Gilteritinib inhibits Glutamine uptake and utilization in FLT3-ITD-positive AML. *Mol Cancer Therapeut* 2021;**20**: 2207−17.
34. Felmlee MA, Jones RS, Rodriguez-Cruz V, Follman KE, Morris ME. Monocarboxylate transporters (SLC16): function, regulation, and role in health and disease. *Pharmacol Rev* 2020;**72**:466−85.
35. Tian HP, Xiao ZX, Su BW, Li YX, Peng H, Meng CY. Impact of SLC16A8 on tumor microenvironment and angiogenesis in colorectal

cancer: new therapeutic target insights. *World J Gastrointest Oncol* 2025;**17**:99188.
36. Zhu R, Ye X, Lu X, Xiao L, Yuan M, Zhao H, et al. ACSS2 acts as a lactyl-CoA synthetase and couples KAT2A to function as a lactyltransferase for histone lactylation and tumor immune evasion. *Cell Metab* 2025;**37**:361-76.e7.
37. Lin Y, Lin A, Cai L, Huang W, Yan S, Wei Y, et al. ACSS2-dependent histone acetylation improves cognition in mouse model of Alzheimer's disease. *Mol Neurodegener* 2023;**18**:47.
38. Xie Y, Hu H, Liu M, Zhou T, Cheng X, Huang W, et al. The role and mechanism of histone lactylation in health and diseases. *Front Genet* 2022;**13**:949252.
39. Iozzo M, Pardella E, Giannoni E, Chiarugi P. The role of protein lactylation: a kaleidoscopic post-translational modification in cancer. *Mol Cell* 2025;**85**:1263−79.
40. Zhang D, Tang Z, Huang H, Zhou G, Cui C, Weng Y, et al. Metabolic regulation of gene expression by histone lactylation. *Nature* 2019;**574**: 575−80.
41. Liberti MV, Locasale JW. Histone lactylation: a new role for glucose metabolism. *Trends Biochem Sci* 2020;**45**:179−82.
42. Ma Z, Yang J, Jia W, Li L, Li Y, Hu J, et al. Histone lactylation-driven B7-H3 expression promotes tumor immune evasion. *Theranostics* 2025;**15**:2338−59.
43. Cortes J. Quizartinib: a potent and selective FLT3 inhibitor for the treatment of patients with FLT3-ITD-positive AML. *J Hematol Oncol* 2024;**17**:111.
44. Al-Kali A, Tibes R, Atherton P, Palmer J, Alkhateeb HB, Patnaik M, et al. A phase II study of combination daunorubicin, cytarabine (Ara-c), and nilotinib (TAsigna) (DATA) in patients newly diagnosed with acute myeloid leukemia with KIT expression. *Am J Hematol* 2023;**98**:472−80.
45. Békés M, Langley DR, Crews CM. PROTAC targeted protein degraders: the past is prologue. *Nat Rev Drug Discov* 2022;**21**:181−200.
46. Zhu H, Wang J, Zhang Q, Pan X, Zhang J. Novel strategies and promising opportunities for targeted protein degradation: an innovative therapeutic approach to overcome cancer resistance. *Pharmacol Ther* 2023;**244**:108371.
47. Cao S, Ma L, Liu Y, Wei M, Yao Y, Li C, et al. Proteolysis-targeting chimera (PROTAC) modification of dovitinib enhances the antiproliferative effect against FLT3-ITD-positive acute myeloid leukemia cells. *J Med Chem* 2021;**64**:16497−511.
48. Han X, Zhao L, Xiang W, Miao B, Qin C, Wang M, et al. Discovery of ARD-2051 as a potent and orally efficacious proteolysis targeting chimera (PROTAC) degrader of androgen receptor for the treatment of advanced prostate cancer. *J Med Chem* 2023;**66**:8822−43.
49. Wang Y, Wang M, Ma L, Zhang Y, Jiao Y, Zhang S, et al. Identification of a potent and selective CDK9 degrader as a targeted therapeutic option for the treatment of small-cell lung cancer. *J Med Chem* 2025;**88**:2528−50.
50. Hu J, Jarusiewicz J, Du G, Nishiguchi G, Yoshimura S, Panetta JC, et al. Preclinical evaluation of proteolytic targeting of LCK as a therapeutic approach in T cell acute lymphoblastic leukemia. *Sci Transl Med* 2022;**14**:eabo5228.
51. Azman M, Sabri AH, Anjani QK, Mustaffa MF, Hamid KA. Intestinal absorption study: challenges and absorption enhancement strategies in improving oral drug delivery. *Pharmaceuticals* 2022;**15**:975.
52. Lee SH, Lopes de Menezes D, Vora J, Harris A, Ye H, Nordahl L, et al. *In vivo* target modulation and biological activity of CHIR-258, a multitargeted growth factor receptor kinase inhibitor, in colon cancer models. *Clin Cancer Res* 2005;**11**:3633−41.
53. Böhmer FD, Karagyozov L, Uecker A, Serve H, Botzki A, Mahboobi S, et al. A single amino acid exchange inverts susceptibility of related receptor tyrosine kinases for the ATP site inhibitor STI-571. *J Biol Chem* 2003;**278**:5148−55.
54. Tran TH, Nguyen JV, Stecula A, Akutagawa J, Moorman AV, Braun BS, et al. The EBF1-PDGFRβ T681I mutation is highly resistant to imatinib and dasatinib *in vitro* and detectable in clinical samples prior to treatment. *Haematologica* 2021;**106**:2242−5.
55. Daver N, Schlenk RF, Russell NH, Levis MJ. Targeting FLT3 mutations in AML: review of current knowledge and evidence. *Leukemia* 2019;**33**:299−312.
56. Wang J, Rong Q, Ye L, Fang B, Zhao Y, Sun Y, et al. Discovery of a novel orally bioavailable FLT3-PROTAC degrader for efficient treatment of acute myeloid leukemia and overcoming resistance of FLT3 inhibitors. *J Med Chem* 2024;**67**:7197−224.
57. Zhou J, Gu J, Qian Q, Zhang Y, Huang T, Li X, et al. Lactate supports Treg function and immune balance *via* MGAT1 effects on *N*-glycosylation in the mitochondria. *J Clin Investig* 2024;**134**:e175897.
58. Singh M, Afonso J, Sharma D, Gupta R, Kumar V, Rani R, et al. Targeting monocarboxylate transporters (MCTs) in cancer: how close are we to the clinics?. *Semin Cancer Biol* 2023;**90**:1−14.
59. Grisolano JL, O'Neal J, Cain J, Tomasson MH. An activated receptor tyrosine kinase, TEL/PDGFbetaR, cooperates with AML1/ETO to induce acute myeloid leukemia in mice. *Proc Natl Acad Sci U S A* 2003;**100**:9506−11.
60. Wang Z, Liu T, Liu W, Gao X, Wan L, Qiu S, et al. A novel subclonal rearrangement of the STRN3::PDGFRβ gene in de novo acute myeloid leukemia with NPM1 mutation and its leukemogenic effects. *Cancer Gene Ther* 2023;**30**:1471−84.
61. Xu R, Du A, Li J, Yang Q. An anoikis-related gene signature predicts prognosis in patients with acute myeloid leukemia and immunotherapy. *Am J Cancer Res* 2024;**14**:5116−32.
62. Xiao Q, Lei L, Ren J, Peng M, Jing Y, Jiang X, et al. Mutant NPM1-regulated FTO-mediated m6A demethylation promotes leukemic cell survival *via* PDGFRβ/ERK signaling axis. *Front Oncol* 2022;**12**: 817584.
63. Mathias TJ, Natarajan K, Shukla S, Doshi KA, Singh ZN, Ambudkar SV, et al. The FLT3 and PDGFR inhibitor crenolanib is a substrate of the multidrug resistance protein ABCB1 but does not inhibit transport function at pharmacologically relevant concentrations. *Invest N Drugs* 2015;**33**:300−9.
64. Naymagon L, Marcellino B, Mascarenhas J. Eosinophilia in acute myeloid leukemia: overlooked and underexamined. *Blood Rev* 2019; **36**:23−31.
65. Ikezoe T, Nishioka C, Tasaka T, Yang Y, Komatsu N, Togitani K, et al. The antitumor effects of sunitinib (formerly SU11248) against a variety of human hematologic malignancies: enhancement of growth inhibition *via* inhibition of mammalian target of rapamycin signaling. *Mol Cancer Therapeut* 2006;**5**:2522−30.
66. Kelly LM, Yu JC, Boulton CL, Apatira M, Li J, Sullivan CM, et al. CT53518, a novel selective FLT3 antagonist for the treatment of acute myelogenous leukemia (AML). *Cancer Cell* 2022;**1**:421−32.
67. Di Giacomo D, Quintini M, Pierini V, Pellanera F, La Starza R, Gorello P, et al. Genomic and clinical findings in myeloid neoplasms with PDGFRβ rearrangement. *Ann Hematol* 2022;**101**:297−307.